LAWRENCE
LIVERMORE
NATIONAL
LABORATORY

LLNL-TR-825574

M4SF-21LL010302052-Steel Corrosion Impacts on Radionuclide Immobilization

E. Balboni, M. Zavarin, K. Smith, C. Booth

August 9, 2021

Disclaimer

This work performed under the auspices of the U.S. Department of Energy by Lawrence Livermore National Laboratory under Contract DE-AC52-07NA27344.

July 16, 2021

M4SF-21LL010302052-Steel Corrosion Impacts on Radionuclide Immobilization

E. Balboni[1], M. Zavarin[1], K. Smith[2], C. Booth[2]

[1] Glenn T. Seaborg Institute, Physical & Life Sciences, Lawrence Livermore National Laboratory, 7000 East Avenue, Livermore, CA 94550, USA.
[2] Lawrence Berkeley National Laboratory, One Cyclotron Road, Mailstop 70A1150, Berkeley, CA 94720
USA

DISCLAIMER

Contents

1. Introduction

This progress report (Level 4 Milestone Number M4SF-21LL010302052) summarizes research conducted at Lawrence Livermore National Laboratory (LLNL) within the Crystalline Activity Number SF-21LL01030205. The research is focused on actinide and radionuclide sequestration in steel corrosion products.

Fuel matrix degradation models suggest that the near field is likely to be reducing at the time of canister breaching, steel corrosion, and radionuclide release, but more oxidizing conditions may prevail in the far field. The incorporation of radionuclides into corrosion phases may limit the rate of radionuclide release by sequestering a portion of the radionuclide source term. For these reasons there is a need to evaluate the incorporation of Pu and other radionuclides into various Fe-oxide phases, and to understand the behavior of coprecipitated phases during mineral recrystallization processes and during re-oxidation events. Radionuclide coprecipitation with Fe minerals may impact long-term repository performance and is an ongoing research focus at Lawrence Livermore National Laboratory.

The effort described in this document includes:

- A summary of the paper "*Transformation of ferrihydrite to goethite and the of plutonium*" published in October 2020 in Earth and Space Chemistry
- A summary of the paper "*Plutonium coprecipitation with calcite*". This paper was submitted to earth and Space Chemistry on June 6th 2021 and we are currently working on addressing reviewer's comments.

In FY21, we continued our effort started in FY20 on performing an assessment to identify the most critical radionuclides and data gaps associated with radionuclide interaction with corrosion products. The overall goal of the effort is to summarize how radionuclides are expected to interact with Fe minerals relevant for the safety assessment of a geological repository. The radionuclides of interest we identified include Tc, Se, Np, Pu and I. In our FY20 report we included literature review on Se and Tc interactions with various Fe minerals. In this FY21 report, we completed our literature review on Np, Pu and I.

Additionally, to gain a comprehensive understanding of coprecipitation behavior with Fe minerals, we calculated partition coefficients (λ_{Me}) using data found in our literature review. Our results show that λ_{Me} provides a valid approach to describe radionuclide coprecipitation behavior from data sourced from the literature. We plan to submit a summary of our findings to a special issue of the journal Minerals "*Formation, Fate and Transformation of Toxic Heavy Metal Minerals (U, Pb, As, Cr, Se and Hg) in the environment*" (drafts due October 2021).

2. Tranformation of ferrihydrite to goethite and the fate of plutonium

Balboni, E., Smith, K.F., Moreau, L., Li, T.T., Booth, C., Maloubier, M., Kersting, A.B., Zavarin, M. Transformation of ferrihydrite to goethite and the fate of plutonium. **ACS Earth Space Chem. 2020,** 4, 11, 1993–2006 (Figure 1)

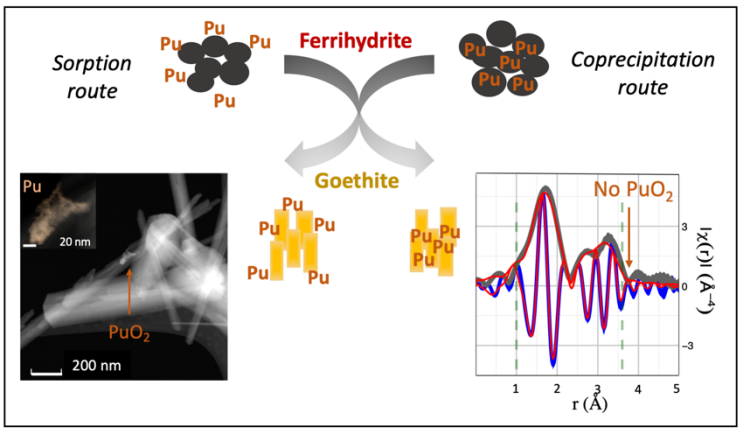

Figure 1 Graphical abstract of "transformation of ferrihydrite to goethite and the fate of plutonium"

Understanding the interactions between plutonium and iron (oxy)hydroxide minerals is necessary to gain a predictive understanding of plutonium environmental mobility and to evaluate long-term performance of nuclear waste repositories. We investigated the fate of plutonium during the formation of ferrihydrite and its subsequent transformation into goethite. Ferrihydrite was synthesized with varying quantities of Pu(IV) following either a sorption or coprecipitation process; the ferrihydrite was then aged hydrothermally to yield goethite. The synthesized materials were characterized via extended X-ray absorption fine structure spectroscopy, transmission electron microscopy, and acid leaching to elucidate the nature of plutonium association with ferrihydrite and goethite. In samples prepared following the sorption method, plutonium was identified in two different forms: a PuO_2 precipitate and a surface-sorbed plutonium complex. For the samples prepared via coprecipitation, no PuO_2 formation occurs in the ferrihydrite precursor and in the goethite experiments where plutonium concentration is ≤1000 ppm (mg kg^{-1}). In these coprecipitation products, plutonium is strongly bound to the minerals either via formation of an inner sphere complex, or via an incorporation process. In the coprecipitation experiments, PuO_2 formation only occurs at the highest plutonium concentration (3000 ppm), suggesting that during ferrihydrite transformation into goethite, part of the plutonium can be remobilized to form PuO_2 nanoparticles. Collectively, our results demonstrate that the nature of plutonium associated with the precursor ferrihydrite (adsorbed vs coprecipitated) will have a direct impact on the association of plutonium with its alteration product (goethite). Furthermore, the data illustrate that some properties of plutonium association with the precursor ferrihydrite are retained through the transformation into goethite. These findings show that plutonium strongly associates with iron (oxy)hydroxides formed through coprecipitation processes and in these materials, plutonium can be strongly retained by the iron minerals.

3. Plutonium coprecipitation with calcite

Enrica Balboni, Kurt F. Smith, Liane M. Moreau, Josh Wimpenny, Corwin H. Booth, Annie B. Kersting, Mavrik Zavarin, Submitted on 06/02/2021 to ACS Earth and Space Chemistry. Reviews received on 06/28/2021 and due 08/11/2021 (Figure 2)

Summary of reviewer's comments: Reviews were for the most part positive. The reviewers requested more detailed about the laser ablation data (analytical settings and calculation of Pu ppm) and some additional clarifications about XAS data (in particular about the XANES component).

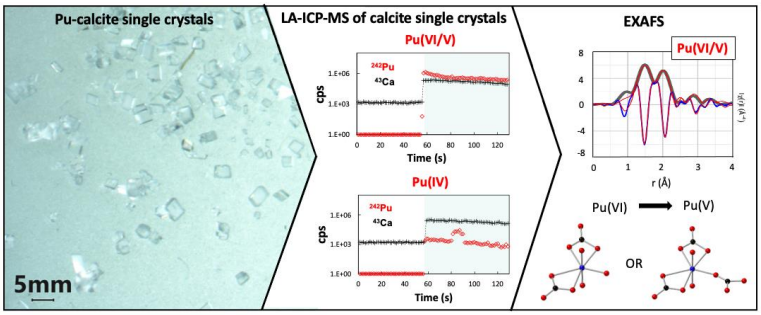

Figure 2 Graphical abstract for "Plutonium coprecipitation with calcite"

The mobility of plutonium (Pu) in the subsurface is affected by Pu-mineral interactions such as adsorption-desorption and structural incorporation. Calcite ($CaCO_3$) is a common secondary phase in near surface environments and a major component of many rocks and soils. In geological repositories, calcite is expected to form as an alteration product of cement-based materials. The reactivity of the calcite surface and its ability to tolerate significant variations in its chemical composition through substitution of Ca for other cations make calcite a potentially important sink for environmental contaminants. Here, single crystals of calcite were synthesized from aqueous solutions containing Pu either as Pu(VI) or Pu(IV) and characterized using a combination of laser ablation inductively coupled plasma mass spectrometry (LA-ICP-MS) and x-ray absorption spectroscopy (XAS). These data are used to assess the amount, structure, and oxidation state of Pu coprecipitated into calcite, providing insight into the potential for Pu sequestration in calcite precipitates. Overall, the XAS and LA-ICP-MS data support the coprecipitation of plutonyl (PuVI/V) in the bulk calcite, though the exact nature of the complex is difficult to elucidate. The coprecipitated plutonyl could be either incorporated in distorted Ca lattice sites or in defect sites. We provide evidence to suggest that Pu(VI) is reduced to Pu(V) during calcite synthesis, but no further reduction to Pu(IV) is observed. The LA-ICP-MS additionally shows that the coprecipitation of Pu(VI/V) is favored over the coprecipitation of Pu(IV). Overall, our results suggest that Pu sequestration in calcite under environmental conditions could immobilize Pu and isolate it from groundwater interactions in contaminated environments and nuclear waste repositories.

3.1 Methods

Single crystals of calcite were synthesized from aqueous solutions containing Pu either as Pu(VI) or Pu(IV). We selected a synthesis method that yields calcite single crystals that are tens to hundreds of micrometers in size (Balboni et al., 2015; Fernelius and Detling, 1934). The quantity of Pu introduced in the syntheses was aliquoted to obtain final calcite samples with 1500 or 700 ppm of Pu (described throughout as PuVI-1500 and PuVI-700 experiments). A calcite synthesis without addition of Pu was also performed (Pu-free experiment). Calcite crystals were isolated and characterized using a combination of laser ablation inductively coupled plasma mass spectrometry (LA-ICP-MS) and x-ray absorption spectroscopy (XAS). These data are used to assess the amount, structure, and oxidation state of Pu coprecipitated into calcite, providing insight into the potential for Pu sequestration in calcite precipitates. Powder x-ray diffraction was used to characterize the purity of the synthetic product, and speciation modeling (PHREEQC 3.6.2 in conjunction with the Specific Interaction Theory (SIT) ANDRA/RWM ThermoChimie-TBD database) was carried out to help us determine the Pu speciation in the synthesis solutions.

3.2 Results and discussion

Synthesis

Due to the dynamic nature of the synthesis method chosen for this work, crystals nucleate and grow at different rates, as the pH and reactant concentrations change. If Pu is incorporated into the growing calcite crystals in any appreciable quantity, its concentration in the aqueous solution will decrease through time. Analysis of aliquots of the barrier solutions for the PuVI-1500 and PuVI-700 experiments sampled over time (1, 2, 3, 4, 8, 9, and 12 days) reveals a decrease in the Pu concentration starting at day 3, at which time crystals have started to form (Figure 3). After 12 days, approximately 30 and 15% of Pu remains in the barrier solution in the PuVI-1500 and PuVI-700 experiments, respectively. The uptake of Pu by calcite is slower and more gradual than reported for Np(V)-doped calcite grown in similar synthetic conditions (complete Np(V) uptake within 3 days) (Balboni et al., 2015). On the other hand, the uptake of Pu(VI) seems somewhat more favorable than for U(VI), as coprecipitation experiments conducted under similar experimental conditions show that U(VI) uptake is slow and gradual, and that 70-80 % of U(VI) remain in solution after calcite crystallization (Balboni et al., 2015).

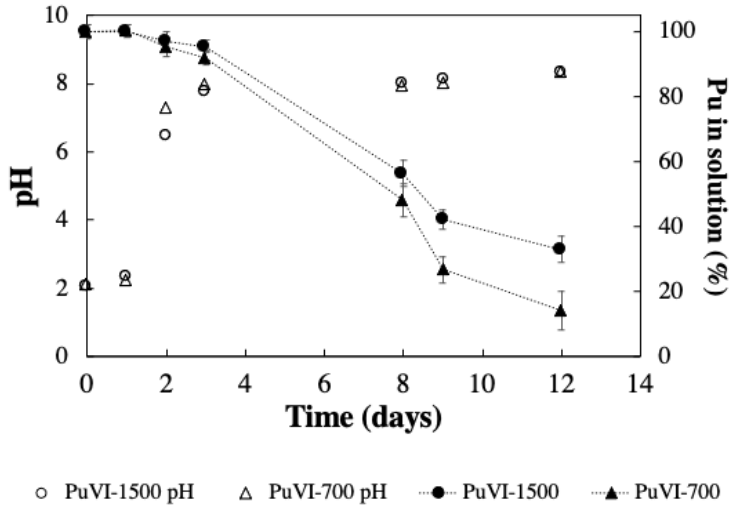

Figure 3 Evolution of pH and Pu during the synthesis of calcite with Pu-1500 (circles) and Pu-700 (triangles).

Lanthanum fluoride precipitation of the barrier solution sampled at day 1, 2, 3, 8, 9, and 12 showed that greater than 90% of Pu is present as Pu(V/VI) in solution in the PuVI-700 experiment. In the PuVI-1500 experiment, greater than 94% of Pu is present as Pu(V/VI) at all sampling days with a slight decrease at day 12, where the percentage of Pu(V/VI) decreased to ≈77%. The oxidation state data demonstrate that the aqueous Pu in both the PuVI-1500 and PuVI-700 experiments remains in the higher oxidation states (V/VI) throughout the duration of the mineral synthesis. The pH profile measured for PuIV-1500 is similar to that of PuVI-1500 and PuVI-700 (included in supplementary information of submitted paper).

LA-ICP-MS

The slow nucleation and growth of crystals in the apparatus allows the crystallization of single crystals of calcite that are tens to hundreds of micrometers in size (Figure 4a). LA-ICP-MS analyses of single crystals are invaluable for demonstrating actinide incorporation (or the lack thereof) within the target crystal, as depth-dependent LA-ICP-MS data provide an indication of the homogeneous or heterogeneous nature of actinide incorporation (Balboni et al., 2015; Klingensmith and Burns, 2007). In this work the crystals were mounted in epoxy and polished through their midplane (Figure 4b), and as such the LA-ICP-MS results can provide strong evidence of Pu coprecipitation within the calcite crystal. Due to the nature of the synthesis setup, a range of Pu incorporation levels is expected, thus fluctuations of the count rate during LA-ICP-MS measurements potentially reflect compositional variations and sample ablation-rate variability. One depth profile laser ablation data was obtained for 15 crystals for PuVI-1500, PuVI-700 and PuIV-1500, and for 3 calcite crystals synthesized in the absence of Pu (Pu-free) (Figure 5 and additional figures in supplementary information submitted with paper).

Figure 5 shows examples of two LA-ICP-MS depth profiles for ^{242}Pu and ^{43}Ca from single calcite crystals selected from experiment PuVI-1500 and PuIV-1500. For the PuVI-1500 sample (Figure 5a) after a background count of 60 s, the laser struck the sample, and immediately counts in the 242 and 43 mass windows are detected. The counts in the 242 window, that correspond to Pu remain fairly constant during the 60 second ablation period, confirming coprecipitation of Pu in the calcite crystal. All measured crystals for PuVI-1500 and PuVI-700 display similar trends. The LA-ICP-MS results can be used to estimate an upper limit for Pu incorporation. To estimate the maximum Pu incorporation, the counts per second measured for Pu are compared to the counts measured for ^{43}Ca in calcite: the known concentration of ^{43}Ca in the synthetic calcite permit estimation of the concentration of Pu. Results show that calcite crystals isolated from experiment PuVI-1500 incorporate on average 600 ppm of Pu, with a minimum of 200 ppm Pu and a maximum of 2700 ppm of Pu detected in each crystal examined by LA-ICP-MS. The uptake of Pu by crystals isolated from PuVI-700 is slightly lower with an average of 350 ppm ranging between 0-850 ppm. The level of Pu coprecipitated within the PuVI-1500 and PuVI-700 experiments is consistent with the reported range of Np(V) (400-1000 ppm) and U(VI) (0-150 ppm) synthesized under similar conditions [10].

An example of the laser ablation depth profiling pattern for a crystal selected from experiment PuIV-1500 is shown in Figure 5b. The ^{43}Ca counts in PuIV-1500 (Figure 5b) are comparable in intensity to those of PuVI-1500 (Figure 5a); however, the Pu signal shows a different trend. The ^{242}Pu counts from PuIV-1500 are up to an order of magnitude lower than in PuVI-1500 and are noisier with signal fluctuations at 80 and 110 s. Similar laser ablation patterns (low counts, signal fluctuations) are observed for other calcite crystals isolated from PuIV-1500. The amount of Pu coprecipitated in calcite crystals isolated from PuIV-1500 ranges between 2-370 ppm (average 100 ppm) and is overall lower than estimates for PuVI-1500 and PuVI-700. This value is somewhat consistent with the amount of U(IV) found in natural calcite crystals (5-35ppm) (Sturchio et al., 1998). The signal fluctuations in the laser ablation pattern of crystals isolated from PuIV-1500 (Figure 5b) could be consistent with the ablation of occluded Pu-phases present in the calcite bulk crystal. For example, thermodynamic calculations indicate that a Pu(IV) precipitates could precipitate in the PuIV-1500 experiments. As the calcite crystals grow in the PuIV-1500 experiment, Pu precipitate particles may be taken up by calcite crystals as an occluded phase, possibly manifesting during laser ablation depth profiling data as Pu-rich particles are ablated by the laser.

The ^{43}Ca counts collected in the Pu-free calcite are comparable in intensity to the counts measured in PuVI-1500, PuVI-700 and PuIV-1500; however as expected no signal in the 242 mass window is detected.

Overall, the LA-ICP-MS data clearly show that the uptake of Pu from calcite synthesized from Pu(VI) solutions is favored, and that Pu(VI) solutions yield calcite crystals with Pu uniformly coprecipitated in the calcite bulk. The uptake of Pu from calcite synthesized from Pu(IV) solutions is less favorable than Pu(VI), forms a more heterogeneous distribution of Pu in calcite, and may reflect the formation of occluded Pu precipitates.

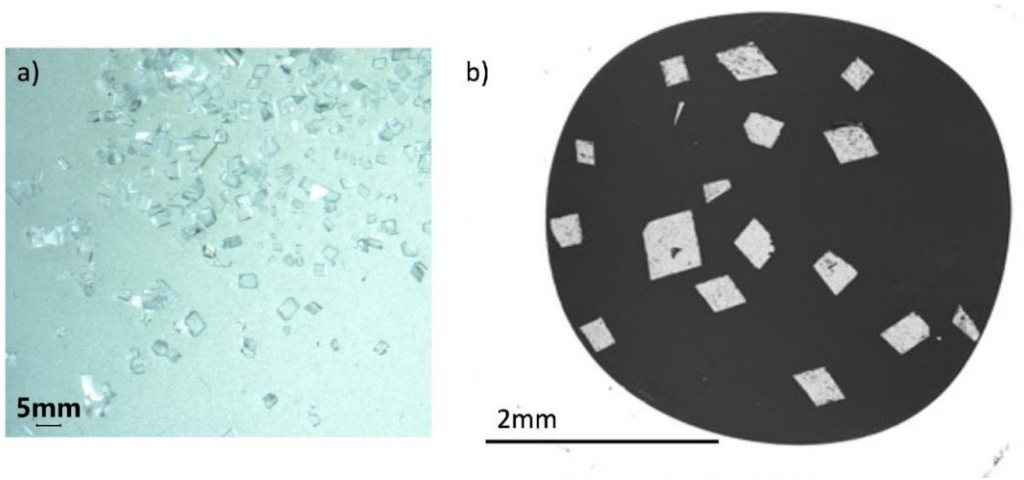

Figure 4 optical image of calcite crystals (Pu-free); b) scanning electron microscope backscatter electron image of calcite crystals embedded in epoxy and polished through mid-plane (Pu-VI 1500)

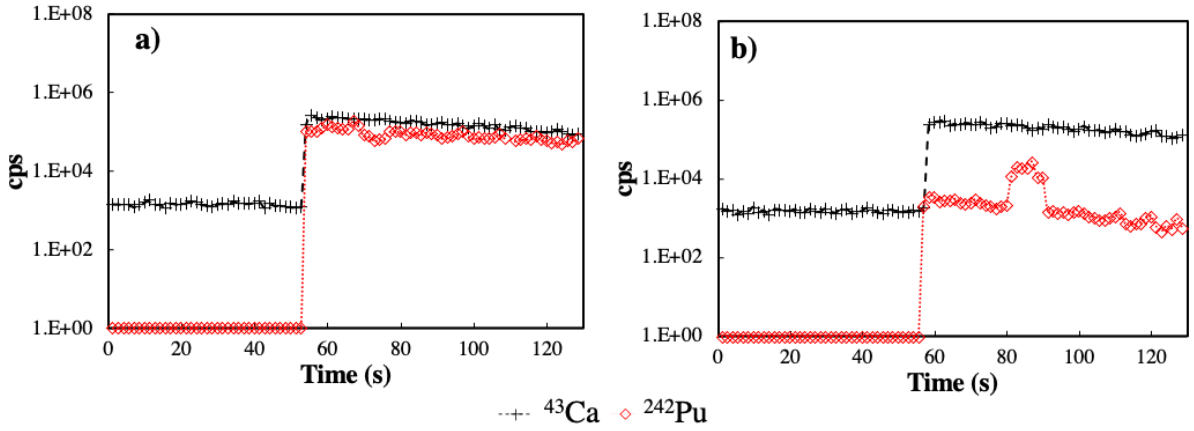

Figure 5 Two examples of a LA-ICP-MS transect for ^{43}Ca and ^{242}Pu prior to laser ablation (0-60s) and during laser ablation depth profiling (60-120s) of calcite crystals from the a) PuVI-1500 and b) PuIV-1500 experiments. Additional examples of laser ablation patterns for calcite crystals isolated from PuVI-1500, PuVI-700, PuIV-1500 and Pu-free can be found in the supplementary information.

X-ray absorption spectroscopy

The PuVI-1500 material was characterized using XAS. The x-ray absorption near-edge structure (XANES) spectrum exhibits a strong shoulder at ≈ 18090 eV demonstrating Pu is present predominantly as plutonyl ($Pu(V)O_2^+$ or $Pu(VI)O_2^{2+}$). The presence of either oxidation state of Pu is plausible given the known sensitivity of Pu to spontaneous redox transformations, particularly in the presence of mineral surfaces (Hixon and Powell, 2018; Shaughnessy et al., 2003; Zhao et al., 2016). However, no evidence of further

reduction to Pu(IV) is observed. Unfortunately, the Pu concentrations in the other experiments (PuVI-700 and PuIV-1500) were too low for XAS analysis.

The background subtracted Pu L_{III}-edge EXAFS spectrum ($k^3\chi(k)$ as a function of the photoelectron wave vector k) and corresponding Fourier transform (FT) for PuVI-1500 are shown in Figure 6. The EXAFS FT shows four distinct features at $r \approx 1.45$, 2.0, 2.9 and 3.25 Å. Note that we refer to the x-axis of the FT as r, which differs from pair distances (R) due to known photoelectron phase shift effects.

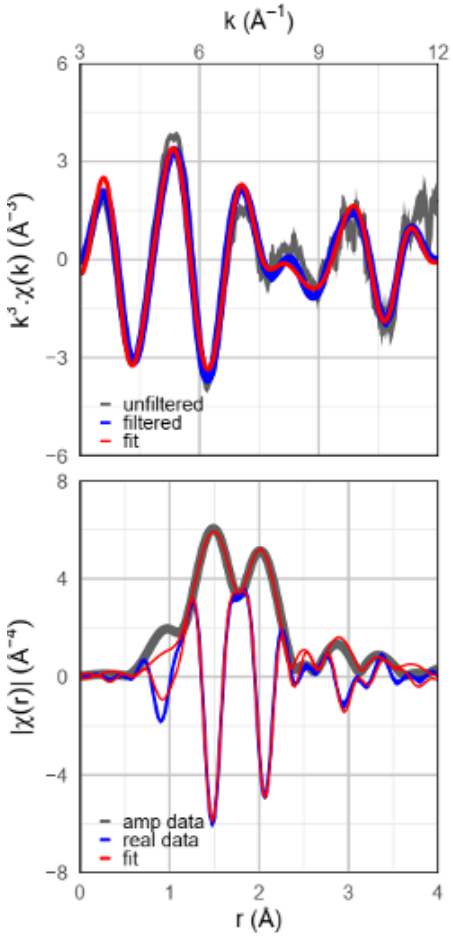

Figure 6 Pu L_{III}-edge EXAFS data and fit results for PuVI-1500 measured at 30 K. Top: EXAFS results in k-space. Bottom: corresponding FT of the k-space data and fit (triscarbonato model). Data were transformed between 3 and 12 $Å^{-1}$ using a Gaussian window with a width of 0.3 $Å^{-1}$ and data were fit between 1.2 and 4 Å. The raw unfiltered data error bars (encompassed by the solid gray shaded area around the data set) were estimated by the standard deviation of the mean between traces.

Initial fits determined that a minimum of four scattering shells were required to adequately describe the data. It is difficult to differentiate between C and O backscattering atoms using EXAFS, so we assigned the species and other labels based on chemical knowledge, discussed further below. The four shells used were: a short (axial)

oxygen shell, Pu-O_{ax} at 1.81 ± 0.01 Å; two shells of equatorial oxygens, Pu-O_{eq1} and Pu-O_{eq2}, at about 2.22 ± 0.02 Å and 2.40 ± 0.01 Å, respectively; and a longer carbon shell, Pu-C, at about 3.31 ± 0.02 Å. The apparent split in the Pu-O_{eq} shell of $\Delta_R \approx 0.2$ Å is significantly larger than the spatial resolution of the EXAFS data ($\delta_r = 0.5\pi/k_{max} = 0.13$ Å). Furthermore the presence of a split Pu-O_{eq} shell is also supported by an F-test with 99.5% probability (Downward et al., 2007). Full details of this fit, noted as "unconstrained", are reported in Table 1.

A Pu-O_{ax} bond distance of 1.81 Å broadly correlates with other studies on actinyl (U, Np) incorporation into the calcite structure (Heberling et al., 2008; Kelly et al., 2006; Reeder et al., 2000; Reeder et al., 2001; Smith et al., 2015). Interestingly, a Pu-O_{ax} interatomic distance of 1.81 Å is elongated compared to the expected Pu(VI)-O_{ax} interatomic distances (1.72 - 1.78 Å (Conradson et al., 2004; Pidchenko et al., 2020; Runde et al., 2003; Wang et al., 2011)), but is consistent with expectations for the Pu(V) moiety (PuO_2^+), with reported interatomic distances of 1.81-1.82 Å for solid compounds (Kvashnina et al., 2019) and aqueous complexes (Conradson et al., 2004; Dalodiere et al., 2018; Di Giandomenico et al., 2009; Panak et al., 2002). The possible presence of Pu(V) is also supported by the elevated Debye Waller factor (σ^2) of 0.010 ± 0.001 $Å^2$ (Table 1, unconstrained model) which suggest there may be some splitting of the Pu-O_{ax} environment within the resolution of the EXAFS data consistent with a mixed Pu(V/VI) system. Given the enhanced Debye-Waller factor, and the elongated Pu-O_{ax} average bond distance, it is likely that a large proportion of Pu(VI) has undergone reduction to Pu(V). Unfortunately, the L_{III}-edge XANES data cannot help in differentiating between Pu(VI) and Pu(V) due to the close edge energies of the two oxidation states (Allen et al., 1997) so the oxidation state of coprecipitated Pu cannot be conclusively determined.

Four different models were created to describe the EXAFS data: a triscarbonato model; an unconstrained model; a bidentate model and a combined model (Table 1; Figure 7). To guide the modeling and understanding of the Pu EXAFS data we first considered the Pu(VI) and Pu(V) aqueous speciation predicted by our thermodynamic modeling. At the beginning of the experiment (pH 2, mixing fraction < 0.25), the $PuO_2^{2+/+}$ free ions are likely to be dominant in solution. In the Pu(V) thermodynamic model, $PuO_2CO_3^-$ becomes an important species (20-30%) as the mixing fraction approaches 0.5. In the Pu(VI) thermodynamic model, pH has a major effect on the aqueous speciation of Pu(VI) with $PuO_2(CO_3)_2^{2-}$ and $PuO_2CO_{3\,(aq)}$ becoming the dominant aqueous species at higher pH and $PuO_2(CO_3)_3^{4-}$ contributing to ≈ 5% of the aqueous speciation at mixing fractions > 0.75. As Pu carbonate species are expected to be present in the Pu(V/VI) aqueous chemistry in the synthesis solutions, the EXAFS models all assumed the formation of plutonyl carbonate-like complexes.

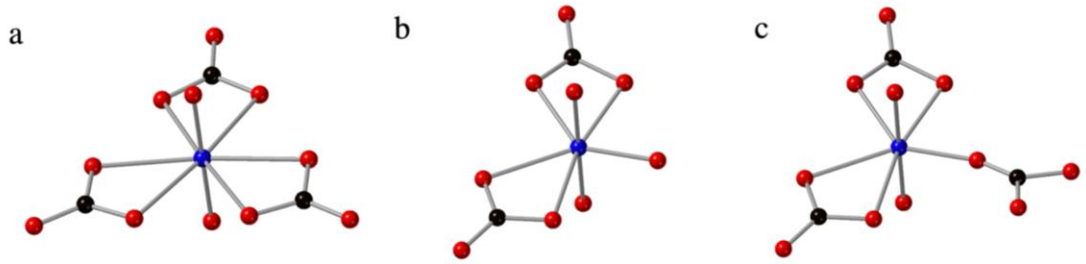

Figure 7 Ball and stick models based on EXAFS data (a) the plutonyl triscarbonato (b) bidentate model (c) combined. Plutonium atoms are in dark blue, oxygen atoms in red, and carbon atoms in black.

Table 1 Summary of EXAFS fits for the PuVI-1500 experiment

Model	**Shell**	**CN**	**R (Å)**	**σ^2 (Å^2)**	**ΔE_0 (eV)**	***R*** **(%)**
triscarbonato	Pu-O_{ax}	2*	1.82(1)	0.010(1)	0.2(2)	11.34
	Pu-O_{eq1}	2*	2.20(2)	0.003(3)†		
	Pu-O_{eq2}	4*	2.39(1)			
	Pu-C	3*	3.33(3)	0.007(4)		
unconstrained	Pu-O_{ax}	2.0*	1.81(1)	0.010(1)	-0.6(2)	9.6
	Pu-O_{eq1}	1.7(3)	2.22(2)	0.002(1)†		
	Pu-O_{eq2}	3.4(5)	2.40(1)			
	Pu-C	1(1)	3.31(2)	0.001(1)		
bidentate	Pu-O_{ax}	2*	1.81(1)	0.010(1)	-0.8(2)	9.6
	Pu-O_{eq1}	1.7(4)	2.22(2)	0.002(1)†		
	Pu-O_{eq2}	3.3(7)	2.40(1)			
	Pu-C	1.7*	3.31(2)	0.001(1)		
combined	Pu-O_{ax}	2*	1.81(1)	0.009(1)	-1.2(2)	11.12
	Pu-O_{eq1}	1.5(3)	2.22(2)	0.001(2)†		
	Pu-O_{eq2}	3.2(6)	2.40(1)			
	Pu-C	3.2*	3.34(3)	0.007(5)		

* indicates a fixed parameter and † indicates a tied σ^2 parameter (i.e. shared in two shells). CN represents the coordination number assuming an amplitude reduction factor of 1; R denotes the interatomic distance; σ^2 represents the Debye Waller factor; ΔE_0 represents the energy shift from the calculated energy Fermi level, and ***R*** (%) is the fit residual.

There are a few factors that we need to consider when evaluating which model is more meaningful in describing the environment of Pu in this sample. For example, the simple triscarbonato model approach implies the incorporation of Pu as a $Pu(VI)(CO_3)_3^{4-}$ and for this sample such incorporation is unlikely to be the case. First, the modeled Pu-O_{ax} distances determined to be 1.81 ± 0.01 Å via EXAFS are indicative of Pu(V) rather than Pu(VI). It is also unlikely for a pentavalent actinide to form a triscarbonato complex (Clark et al., 1995; Dalodiere et al., 2018; Kvashnina et al., 2019; Pidchenko et al., 2020). Finally, coprecipitation studies of U(VI) and Np(V) in calcite have indicated that the actinide triscarbonato complex is unlikely to fit in the calcite structure due to its size and steric hindrance. On consideration of all the different aspects of this modelling we are confident that a plutonyl carbonate complex is dominating Pu speciation in the synthesized calcite and that Pu is coordinated by carbonate ligands in both a mono- and bi-dentate fashion (analogous to the U(VI) carbonate complex of (Reeder et al., 2000)). Furthermore, given our Pu-O_{ax} interatomic distances, we suspect that the majority of Pu(VI) has been reduced to Pu(V) in the process of Pu(VI) coprecipitation with calcite, though the elevated Debye Waller factor in the Pu-O_{ax} shell strongly implies this reduction is not complete leaving a minor, but unquantifiable, component of Pu(VI).

This finding is broadly compatible with plutonyl incorporation into the calcite structure; however without the identification of Ca scatterers it is difficult to independently confirm if Pu is substituting for Ca or is present in defect sites. Previous EXAFS studies of calcite coprecipitated with U(VI) and Np(V) were also unsuccessful in identifying U-Ca and Np-Ca scatterers (Heberling et al., 2008; Reeder et al., 2000; Reeder et al., 2001) and Heberling et al. (Heberling et al., 2008) suggested that the Pu-Ca distance is too long to be identified in their room temperature EXAFS. Reeder et al. (Reeder et al., 2000; Reeder et al., 2001) interpreted the lack of U-Ca scatterers in their study as indicative of a largely disordered environment beyond the nearest equatorial shells. The lack of evidence for any Pu-Pu backscattering in the PuVI-1500 experiment however makes the formation of Pu clusters or the presence of polymeric Pu species unlikely. Furthermore, thermodynamic calculations indicate $PuO_2CO_3(s)$ is not expected to precipitate under these experimental conditions.

3.3 Conclusions

Overall, the LA-ICP-MS and EXAFS data clearly support the coprecipitation of plutonyl in the bulk calcite. There is evidence to suggest that Pu(VI) reduced to Pu(V) during calcite synthesis and that Pu resides in a distorted Ca position in calcite or in defect sites as a Pu(V) carbonate complex. In the experiments that started with Pu(VI) further reduction to Pu(IV) was not observed. The LA-ICP-MS additionally shows that the coprecipitation of Pu(VI) is favored over the coprecipitation of Pu(IV). Regardless of the exact nature of Pu configuration in calcite, it does appear that Pu sequestration in calcite may immobilize Pu and isolates it from groundwater interaction in contaminated environments and nuclear waste repositories.

4. Radionuclide interactions with Fe(II)/(III) minerals

4.1 Neptunium

Neptunium (Np) does not occur naturally in any appreciable quantity (Katz and Hayes, 1995) but is created during the burn up of uranium-based nuclear fuel in commercial reactors for the generation of electricity, and in plutonium-production reactors operated for military purposes. While initially a small contributor to the total activity of a nuclear repository, ^{237}Np is expected to be the major dose contributor after 10,000 years because of its long half-life (2.14 million years) and ingrowth from ^{241}Am decay (Kaszuba and Runde, 1999). Anthropogenic sources of neptunium and americium have been introduced into the environment through nuclear weapons testing and improper disposal at legacy waste sites. For example, underground testing at the Nevada Test Site generated 1.23 x 10^6 TBq of radionuclides, including 1.80 TBq ^{237}Np and 1.37 x10^3 TBq ^{241}Am (Smith et al., 2003); and an estimated 1.06 x 10^3 TBq ^{241}Am and ~2 TBq ^{237}Np were disposed in the near-surface region of the Hanford Site as liquid waste (Cantrell, 2009; Cantrell et al., 2014). The high-toxicity and persistence of ^{237}Np highlights the importance of developing a thorough understanding of the factors controlling its environmental mobility for accurate assessment of nuclear repositories.

Oxidation state and aqueous chemistry

Behaving similar to uranium (U) and plutonium (Pu), neptunium is able to exist in a wide range of oxidation states from +III to +VII , although +IV and +V states are most relevant to natural environments. The coordination geometry of Np depends on the oxidation state: Np(III) and Np(IV) are spherically coordinated ions, whereas Np(V) and Np(VI) form the linear trans-dioxo cations NpO_2^+ and NpO_2^{2+}, which are coordinated by four, five, or six donor atoms of ligands at the equatorial vertices. Aqueous speciation of Np is dominated by the pentavalent neptunyl cation (NpO_2^+) (Kaszuba and Runde, 1999), while the tetravalent neptunium (Np^{4+}) exists under reducing conditions that characterize the subsurface of nuclear waste repositories (Husar et al., 2015).

In acidic matrices, Np redox chemistry is dominated by the dynamic equilibria: NpO_2^{2+} $\Leftrightarrow$ NpO_2^+ $\Leftrightarrow$ Np^{4+} (Chatterjee et al., 2017) with the standard potential of the NpO_2^+/NpO_2^{2+} and Np^{4+}/NpO_2^+ couples being 1.161 ± 0.014 V and 0.596 ±0.078 V, respectively (Cohen and Hindman, 1952; Kaszuba and Runde, 1999; Riglet et al., 1989). This redox mobility makes Np speciation highly dependent on the aqueous solution composition, which can initiate hydrolysis related processes and the formation of coordination complexes disturbing the Np redox equilibrium. (Hennig et al., 2009; Ikeda-Ohno et al., 2008). Owing to its low solubility, Np(IV) is generally considered to be less mobile than Np(V) in a near-neutral aqueous environment (Neck et al., 2001).

Np aqueous complexation and precipitation of Np compounds and their solubility: strategies for Np disposal

Neptunium in unaltered irradiated UO_2 fuel will be tetravalent and may substitute for U(IV) in the fluorite-structure lattice (Finch et al., 1999). However, in oxygenated water pentavalent neptunium, Np(V), is the stable oxidation state (Antonio et al., 2001; Forbes et al., 2008). Np(V) may enter the environment through a variety of pathways that include the processing of irradiated fuels to isolate fissile isotopes for weapons production or to close a nuclear fuel cycle (Bruno and Ewing, 2006), by the alteration of irradiated fuel in a geologic repository (Efurd et al., 1998), and by interaction of water with damaged nuclear fuel subsequent to a reactor core-melt event such as happened at Fukushima, Japan in 2011 (Burns et al., 2012). It is therefore important to understand the range of processes that will impact the transport of Np(V) in the environment.

Kaszuba and Runde (Kaszuba and Runde, 1999) evaluated how redox potential and solid-phase stability interact and influence neptunium solubility and aqueous speciation in natural systems. Their work shows that two Np(V) hydroxo complexes, $NpO_2OH(aq)$ and $NpO_2(OH)_2^-$, exist in carbonate-free aqueous systems, whereas $NpO_2(CO_3)_n^{1-2n}$ (n =1-3) is the predominant Np(V) carbonato complexes. The uncharged species $Np(OH)_{4(aq)}$ is the most important Np(IV) hydroxo complex in carbonate-free solutions at pH greater than 4, and Np(IV) carbonate speciation is dominated by the complexes $Np(CO_3)_4^{4-}$ and $Np(CO_3)_5^{6-}$. Additionally carbonate complexation and hydrolysis may occur to form mixed hydroxo-carbonato complexes (Kaszuba and Runde, 1999).
In the absence of carbonate, NpO_2OH and Np_2O_5 are the stable Np(V) solid phases, while $MNpO_2CO_3 \cdot xH_2O$ and $M_3NpO_2(CO_3)_2$ ($M=Na^+, K^+$) are the stable solid phases in carbonate-bearing systems, depending on the alkali carbonate concentration. $Np(OH)_{4(am)}$ and NpO_2 are the stable Np(IV) solid phases in systems low in carbonate, while Np(IV) carbonates or hydroxo-carbonates are expected to form in carbonate-containing systems. Neptunium solubility decreases in the pH range 10-12 and increases at pH above 12, and both redox potential and $Np(OH)_{4(am)}$ solubility product control soluble neptunium concentrations at neutral pH and Eh between-0.2 and 0.3. Kaszuba and Runde, 1999 conclude that overall Np_2O_5 and $Np(OH)_{4(am)}$ are the stable solids in aquifers of low ionic strength.

Overall, at alkaline pH, the solubility of metal ions including Np(V) and Np(IV) is expected to be low. As a result, many disposal concepts for intermediate level radioactive wastes use grouting with cement, which develops alkaline conditions intended to reduce the mobility and solubility of radionuclides in waste (Cantrell et al., 2014). Where neptunium is an environmental contaminant, it is likely to be present at concentrations that are low enough to preclude the formation of primary neptunium phases such as Np_2O_5 (Curti, 1999; Kaszuba and Runde, 1999). The aqueous transport of Np(V) in trace amounts may be reduced by co-precipitation reaction in subsurface minerals, or by sorption onto their mineral surfaces, amongst other processes, thus the details of the interactions of dissolved Np(V) with minerals may strongly influence its mobility. Consequently, identification and characterization of secondary phases containing neptunium either as a sorbed or co-precipitated species is essential to our understanding of neptunium environmental geochemistry and nuclear waste disposal issues.

Np adsorption studies

The sorption of Np(V) onto various rock materials and minerals including silicates, aluminum oxides, calcite and iron oxides has been widely studied (Baumer and Hixon, 2019; Baumer et al., 2017; Bradbury and Baeyens, 2006; Combes et al., 1992; Del Nero et al., 1998; Girvin et al., 1991; Guckel et al., 2013; Hakanen and Lindberg, 1991; Jain et al., 2007; Kalmykov et al., 2008; Keeney-Kennicutt and Morse, 1985; Khasanova et al., 2007; Kohler et al., 1999; Mironenko et al., 2006; Muller et al., 2009; Muller et al., 2015; Nakata et al., 2000, 2002, 2004; Schmeide and Bernhard, 2010; Tinnacher et al., 2011; Tochiyama et al., 1996; Turner et al., 1998; Wu et al., 2009; Wylie et al., 2016; Yang et al., 2015; Zavarin et al., 2005).

Li and Kaplan (Li and Kaplan, 2012) reviewed the sorption percentage and sorption coefficients (Kd) of Np sorption onto hematite, magnetite, goethite and ferrihydrite under different conditions (e.g., pH, initial Np concentration, ion strength, sorbent loading, and equilibrium time). Their reviews shows that Np(V) interact with the surface of various Fe oxides, with distribution coefficients as high as 10^5 ml/g (Li and Kaplan, 2012), and we refer to their work for a comprehensive report of Kd values and sorption percentages of Np(V) sorption on iron oxides.

The sorption of Np(IV) and other tetravalent actinides onto mineral surfaces has only been investigated sparingly. Generally, for tetravalent radionuclides (Zr, Hf, Th, U, Np, Pu) a strong sorption onto mineral surfaces has been reported in the absence of additional complexing ligands, such as carbonate or humic material, or other groundwater colloids, (Banik et al., 2007; Nagasaki et al., 1999; Reiller et al., 2002; Sanchez et al., 1985; Takahashi et al., 1999).

Sorption behavior of Np(V)

The sorption of Np(V) onto geological materials, such as montmorillonite, hematite, calcite and kaolinite, has been found to depend on many parameters, such as pH (Zavarin et al., 2005), carbonate concentration (Turner et al., 1998), Np(V) concentration (Mironenko et al., 2006), ionic strength (Kaszuba and Runde, 1999), the concentration of the surface sites (Del Nero et al., 1998), crystal structure, crystallinity, and surface conditions of various oxides and hydrous oxides (Tochiyama et al., 1996). Among these factors, pH and CO_2 are the main parameters that govern the sorption of Np(V). Overall Np(V) sorption to mineral surfaces has been found to be strongly pH-dependent, essentially starting at pH 6 and increasing with increasing pH under carbonate-free conditions. In carbonate-free systems, the molecular speciation of Np(V) sorbed on goethite has been studied by XAS spectroscopy (Combes et al., 1992) and XPS (Teterin et al., 2006). Np LIII-edge EXAFS analysis of the Np/goethite sorption samples showed that Np(V) sorbs as isolated neptunyl (NpO_2^+) groups and not as multinuclear species.

The Np environment consisted of two oxygen shells around Np consisting of two oxygens at 1.85 ± 0.02Å and about five oxygens at 2.51 ± 0.03Å, consistent with a distorted pentagonal-bipyramid complex. A weak feature at ~3Å in the Fourier transforms of the EXAFS spectra was identified as a Np-Fe second-neighbor pair

correlation, which suggested that Np(V) sorbs at the goethite water interface as an inner-sphere complex, rather than as a simple, ordered neptunium oxide or hydroxide or as a co-precipitate.

Under the ambient CO_2 condition, the maximum sorption of Np(V) occurs at nearly neutral pH and the sorption decreases in the alkaline pH region (Del Nero et al., 1998; Li and Tao, 2003; Schmeide and Bernhard, 2010; Turner et al., 1998; Wu et al., 2009), because of the formation of neptunyl carbonate complexes (Kaszuba and Runde, 1999; Wu et al., 2009). An increasing carbonate concentration in the aqueous phase has no effect at pH values below 7 but has been shown to decrease the Np(V) uptake at higher pH values due to formation of stable, weakly sorbing neptunyl carbonate complexes in solution (Kohler et al., 1999; Wu et al., 2009).

Under PCO_2 $10^{-3.5}$ atmosphere, Arai et al. (Arai et al., 2007) investigated Np(V) surface speciation on hematite surfaces at pH 7–9 using XAS. In situ XAS analyses suggested that bis-carbonato inner-sphere and tris-carbonato outer sphere ternary surface species coexist at the hematite-water interface at pH 7–8.8, and the fraction of outer sphere species gradually increases from 27 to 54% with increasing pH from 7 to 8.8.

Effects of organic ligands on Np(V) sorption

Sorption of Np to mineral surface including Fe oxides can be affected by organic ligands (Jain et al., 2007; Khasanova et al., 2007; Schmeide and Bernhard, 2010). For example addition of humic acid (HA) has been shown to enhances the sorption of Np(V) compared to the HA-free system at lower pH which is attributed to Np complexation by HA sorbed onto the mineral surface. At alkaline pH values however, Np(V) sorption is decreased due to the presence of HA. This has been attributed to the formation of soluble Np(V) humate complexes (Niitsu et al., 1997; Pathak and Choppin, 2007; Righetto et al., 1991). In contrast, Jain et al. (Jain et al., 2007) found that under aerobic condition, addition of HA to Np(V)-hematite colloid systems showed little effect on the Np sorption rate at pH 3–6, but slightly decreased the Np sorption rate at pH 6–10; while at anaerobic condition, the addition of HA increased the Np sorption percentage at pH 3–7, but showed little effect on the Np sorption at pH 7–10.

Furthermore, it has been shown that Np(V) is reduced to Np(IV) by humic substances (Schmeide and Bernhard, 2009; Shcherbina et al., 2007; Zeh et al., 1999). The resulting formation of Np(IV) humate complexes strongly increased Np migration through sandy sediment and granitic material columns in laboratory experiments (Artinger et al., 2000; Sakamoto et al., 2000). The impact of redox active humic acids on Np sorption onto goethite has been studied by (Kalmykov et al., 2008). Compared to Np(V), Np sorption strongly increased in the pH range below 5, whereas at higher pH values the Np sorption was slightly decreased due to reduction of Np(V) to Np(IV) by HA.

Np(V) reduction during sorption

Reduction to Np(IV) can also be facilitated by surface interactions with Fe(II) containing minerals, such as magnetite and green rust (Christiansen et al., 2011; Wylie et al., 2016).

Wylie et. al (2016) provide evidence that Ti-substituted magnetite reduces neptunyl species to Np(IV). Their results show that increasing Ti concentration results in higher Np sorption/reduction values at low pH. High-resolution transmission electron microscopy of the Ti-magnetite particles, however, provides no evidence of NpO_2 nanoparticle precipitation. Absence of NpO_2 is confirmed via X-ray absorption spectroscopy analysis of the samples, confirming the nearly exclusive presence of Np(IV) on the titanomagnetite surface. Results also suggest preferential binding of Np to terminal Ti–O sites as opposed to Fe–O sites.

Christiansen et al. (Christiansen et al., 2011) investigated the interaction of NpO_2^+ with green rust sodium sulphate ($GR_{Na,SO4}$). The $GR_{Na,SO4}$ sorbed and reduced NpO_2^+ within minutes and reduced Np(IV) was primarily found as precipitated nanoparticles at the edges of the $GR_{Na,SO4}$ crystal platelets. The position of the particles at the crystal edges suggests initial sorption of Np(V) and subsequent reduction at GR edge sites. During reoxidation experiments in aqueous suspension about 50% of the Np remained associated with the oxidized product and 75% of the associated Np is still present as Np(IV). Bach et al. (2014) characterized the Np nanoparticles formed at the edges of $GR_{Na,SO4}$ via HR-TEM. They identified nanocrystallites of about 2–3.5 nm in size consistent with NpO_2 crystallizing in a fluorite-type structure.

Np coprecipitation process with Fe(II) and Fe(II)/Fe(III) oxy-hydroxides

There is a lack of information on Np(V) incorporation into mineral structures despite the fact that this is potentially a highly effective mechanism to immobilize radionuclide. Bots et al. and Roberts et al. (Bots et al., 2016; Roberts et al., 2019) studied the speciation and fate of neptunium as NpO_2^+ during the crystallization of ferrihydrite to hematite and goethite. The Np(V) stock solution was added to the experiment either at the start of the ferrihydrite crystallization, to assess incorporation processes during crystallization, or to the final crystallization products to assess adsorption processes. Np(V) had a high affinity for the iron(III) (oxyhydr)oxide phases in all experiments with the vast majority of Np(V) (≥96%) sequestered from solution regardless of the experimental systems. The results however showed that adsorption of NpO_2^+ to iron(III) (oxyhydr)oxide phases is reversible and, for ferrihydrite, occurs through the formation of mononuclear bidentate surface complexes. For the adsorption samples, the majority of Np(V) (84−94%) was released during the chemical extraction confirming that Np(V) was predominantly reversibly bound to the surfaces of the iron (oxyhydr)oxides. By contrast, only 6% of the Np(V) was released from the solid phase during the chemical extraction of the pure hematite sample, whereas in mixed hematite/goethite samples crystallized at pH 9.5 and 11, 20-30% of Np(V) remained associated with the solid product after the extraction. Chemical extractions and X-ray absorption spectroscopy (XAS) analyses showed the incorporation of Np(V) into the structure of hematite occurs during its crystallization from ferrihydrite (pH 10.5) through direct replacement of octahedrally coordinated Fe(III) by Np(V) in neptunate-like coordination. Subsequent analyses on mixed goethite and hematite crystallization products (pH 9.5 and 11) showed that Np(V) is incorporated during crystallization, however there is limited evidence for Np(V) incorporation during goethite crystallization at the extreme pH of 13.3. This is likely due to the formation of a Np(V) hydroxide precipitate preventing incorporation into the goethite particles.

Roberts et al. (2019) studied the co-precipitation of Np(V) with Fe(II) bearing iron (oxyhydr)oxides (magnetite and green rust) under anaerobic conditions. During both magnetite and green rust formation, Np(V) was completely removed to solids under the pH 9, mildly alkaline end point. Analysis using chemical extractions and X-ray absorption spectroscopy (XAS) techniques confirmed that Np(V) is initially reduced to Np(IV) during co-precipitation of both magnetite and green rust. Extended X-Ray Absorption Fine Structure (EXAFS) modelling suggested the Np(IV) forms a bidentate binuclear sorption complex to both minerals. Following oxidation in air over several months, ~ 50% the sorbed Np(IV) is partially oxidized to Np(V), but very little remobilization to solution occurs during oxidation.

These two studies show that iron (oxyhydr)oxides have a potential to immobilize Np under both reducing and oxidizing conditions, and that Np is retained through iron (oxyhydr)oxides mineral transformation. Overall reduction of Np(V) to Np(IV), inner sphere sorption and coprecipitation reactions have important implications in understanding the mobility of neptunium in a range of engineered and natural environments.

Np coprecipitation process with other minerals

Various studies have addressed the incorporation behavior of Np(V) in uranyl, carbonate, and sulfate minerals. Briefly, synthetic U(VI) hydroxides and silicates can incorporate various amounts of Np(V) and levels of incorporation are impacted by details of the crystal structure as well as temperature and solution pH under which the compounds form. (Alessi et al., 2013; Burns et al., 2004; Burns and Klingensmith, 2006; Forbes and Burns, 2006) Burns et al., 2004; Burns, 2005; Burns and Klingensmith, 2006; Forbes and Burns, 2006; Alessi et al., 2013). A few studies examined the factors that impact the structural incorporation of the Np(V) neptunyl ions in carbonate and sulfate minerals including calcite ($CaCO_3$) (Balboni et al., 2015; Heberling et al., 2008; Heberling et al., 2011), aragonite ($CaCO_3$), gypsum ($CaSO_4x2H_2O$), strontianite ($SrCO_3$), cerussite ($PbCO_3$), celestine ($SrSO_4$), and anglesite ($PbSO_4$). Amongst the carbonate minerals, calcite significantly favors Np(V) incorporation (Balboni et al., 2015; Heberling et al., 2008; Heberling et al., 2011). Aragonite and strontianite incorporate Np(V) in similar amounts, whereas cerussite does not incorporate Np(V) under the synthesis conditions. Overall, the sulfate minerals weakly interact with the actinyl ions, relative to the carbonate minerals, however incorporation of Np(V) in celestine was observed at the level of a few tens of ppm; whereas anglesite and gypsum did not incorporate detectable Np(V). Geometrical constraints of the Np(V) species in solution, together with the crystallographic steric constraints of the host material, affect preferential uptake in the mineral structures studied. Calcium and strontium appear to be favorable incorporation sites for both Np(V) in aragonite and strontianite.

4.2 Plutonium

Plutonium (Pu) is produced in reactor fuel as a mixture of isotopes. The predominant isotope, ^{239}Pu ($T_{1/2}$= 24 100 years) is produced by neutron capture in ^{238}U. If a fuel element containing ^{239}Pu is left in a reactor for any length of time further neutron capture can occur, yielding isotopes with higher mass, such as ^{240}Pu ($T_{1/2}$= 6560 years), ^{241}Pu ($T_{1/2}$= 14 years), and ^{242}Pu ($T_{1/2}= 3.76\times10^5$ years). In addition, small quantities of two other isotopes, ^{236}Pu ($T_{1/2}$= 2.87 years) and ^{238}Pu ($T_{1/2}$= 87.74 years), are produced during the irradiation of the fuel in normal operating conditions. (OECD, 1989) The isotopes ^{238}Pu, ^{239}Pu, ^{240}Pu, and ^{242}Pu all decay by emission of α-particles, while ^{241}Pu undergoes β decay to produce α and ɣ-emitting ^{241}Am.

The production and testing of nuclear weapons, nuclear accidents, and authorized discharges of radioactive effluents have contributed significantly to Pu contamination in the natural environment. (Geckeis et al., 2019) Pu is also a major constituent in civil and military nuclear wastes and is considered a risk-driving radionuclide in the long-term safety of nuclear waste repositories. Due to the long half-life of some of its isotopes, and radiotoxicity, understanding the mobility of Pu in the environment is a key scientific and societal concern.

Pu Environmental Behavior

A recent review details the environmental behavior of Pu (Geckeis et al., 2019), thus they will be only briefly discussed here. Several factors can influence Pu mobility in the environment including: Pu redox processes (Begg et al., 2018; Choppin, 1991; Sanchez et al., 1985), solubility effects (Efurd et al., 1998; Neck et al., 2007), interactions with natural organic matter (including bacteria) (Icopini et al., 2009; Zhao et al., 2011), and sorption/desorption reactions with mineral surfaces (Begg et al., 2017; Powell et al., 2004; Zavarin et al., 2012). Under typical environmental conditions Pu may exist in the III, IV, V and/or VI oxidation states, each of which demonstrate dramatically different chemical properties (Choppin, 1983; Clark et al., 1995). For example, under environmental conditions the higher oxidation states, V and VI, exist as the highly soluble and mobile PuO_2^{x+} moieties. Although Pu(V) and Pu(VI) predominate under oxic conditions, Pu(IV) is often the most common Pu ion at neutral pH and mildly reducing conditions (Maher et al., 2013). Pu(IV) undergoes rapid hydrolysis in circumneutral environments resulting in a significantly lower solubility than the higher oxidations states, V and VI. Pu hydrolysis reactions may occur at Pu(IV) concentrations > 10^{-8} M (Begg et al., 2015) and result in the formation of discrete $[Pu(OH)_n]^{(4-n)+}$ intrinsic colloids (Dalodiere et al., 2017; Gerber et al., 2020; Maher et al., 2013; Micheau et al., 2020; Moreau et al., 2020; Neck et al., 2007; Powell et al., 2011). At pH >3, the Pu aqueous concentration is dominated by Pu(V) and by the solubility product of Pu(IV) hydrous oxide precipitate. Although Pu(IV) and Pu(V) are the most common oxidation states under circumneutral pH conditions, and both sorb to Pu mineral surfaces, Pu(V) has been shown to reduce to Pu(IV) on surfaces (Begg et al., 2013; Choppin, 1983; Hixon et al., 2010; Kirsch et al., 2011; Powell et al., 2004; Sanchez et al., 1985; Shaughnessy et al., 2003). Moreover, Pu(IV) has a particularly high affinity for iron (oxy)hydroxides mineral surfaces and Fe containing minerals (Begg et al., 2018; Romanchuk et al., 2011; Sanchez et al., 1985; Zhao et al., 2016).

Pu interactions with Fe minerals: sorption, desorption and spectroscopy studies

Pu sorption processes with Fe(III) minerals

Li and Kaplan recently reported a summary on sorption behavior of Pu on various Fe(III) and Fe(II) minerals. Briefly Pu sorption on Fe(II)/(III) oxides is limited at pH < 3 (K_d 7-990 ml/g, sorption <30%) but rapidly increase at neutral pH (K_d 10^4-10^5 ml/g, >90%) (Lu et al., 2003; Powell et al., 2004, 2005; Romanchuk et al., 2011; Runde et al., 2002; Sanchez et al., 1985). These studies highlight that various geochemical factor affect Pu sorption to mineral surfaces including carbonate and organic concentration, Pu concentration, nature of the mineral surfaces, redox reactions, and colloid formation. For example in the presence of dissolved organic carbon (DOC), Pu(V) reduction to Pu(IV) occurs in solution, commonly the result of the presence of the reducing properties of quinones and hydroquinones in the DOC. Pu(IV) sorption on goethite can decrease by 30% in the presence of 240 mg/L natural DOC (Sanchez et al., 1985). Increasing concentrations of carbonate ligands to 100 meq/L (total alkalinity) have little effect on Pu(IV) or Pu(V) sorption to goethite (Sanchez et al., 1985). However, above 100 meq/L total alkalinity, the Pu(IV) and Pu(V) sorption on goethite systematically decrease until essentially all Pu is inhibited from sorption at the carbonate alkalinity ∼1000 meg/L, presumably as a result of the formation of a Pu-CO_3 complexes (Sanchez et al., 1985).

Lu et al. (2003) and Runde et al.(2002) studied the sorption of Pu(V) to hematite in Yucca Mountain J-13 well water (a pH 8, Ca, and carbonate dominated groundwater). Approximately 50–55% of Pu sorb immediately after adding Pu(V) to suspensions containing 1338 m^2/L (25 g/L) colloidal hematite. Over time, the Pu fraction associated with the solid phase slowly increases, until a steady-state was achieved after ∼4 days. Approximately 95% of the Pu is sorbed at a steady-state.

For both goethite (Kersting et al., 2003) and Mn(III) substituted goethite (Hu et al., 2010), Pu LIII-edge XANES spectra of the Pu sorbed samples indicates that oxidized Pu (VI/V) is reduced to Pu(IV) upon contact with the mineral to form an inner-sphere Pu(IV) complex on the mineral surfaces and no evidence of Pu–Pu interactions representing precipitation of Pu(IV) on the goethite surface was found (Hu et al., 2010).

At higher Pu concentration, as Pu(IV) solubility limit increases Pu colloids may precipitate. For example Powell et al. (2011) reported that PuO_2 nanocolloids occurred on goethite surface at pH 7 with an initial Pu(IV) concentrations of ∼1x10^{-6} M. The intrinsic Pu nanocolloids (2–5 nm in diameter) have the expected fcc structure and Fm3m space group, as confirmed by both electron diffraction analysis and high-resolution transmission electron microscopy (HRTEM). However, when a Pu(IV) working solution was gradually added to a synthetic goethite suspension to achieve the final Pu(IV) concentration of 0.99x10^{-6} M, Pu nanocolloids formed on goethite surfaces undergo a lattice distortion relative to the ideal fluorite-type structure, fcc, PuO_2, resulting in the formation of a bcc, Pu_4O_7 structure. This structural distortion results from an epitaxial growth of the Pu colloids on goethite, leading to stronger binding of Pu to goethite.

Pu sorption with Fe(II) containing minerals

Kirsch et al.(2011) investigated the reaction products of aqueous ^{242}Pu(III) and ^{242}Pu(V) reacted with magnetite (Fe_3O_4), mackinawite (FeS), and chukanovite ($Fe_2(CO_3)(OH)_2$) in sorption experiments under anoxic conditions. Results show that Pu concentrations in the liquid phase rapidly go below detection limit. XAS result demonstrate that Pu(V) is reduced in the presence of all three minerals with >90% of the Pu species present as Pu(III), independent of the initial Pu oxidation states. For magnetite the Fourier transform peaks of EXAFS were fitted best with two shells: the first Pu–O peak corresponds to 9 oxygen atoms at 2.49Å and the first Pu–Fe peak to three iron atoms at 3.54 Å. The spectroscopy results exclude formation of a dimeric surface complex or of Pu(III) (hydr)oxide clusters due to the lack of Pu–Pu backscattering in the experimental spectrum. The Pu(III) surface complexation at the octahedrally terminated (111) face is described as a tridentate, trinuclear, triple edge-sharing surface complex. As such, it is likely to be very stable and plays an important role in controlling Pu-magnetite reactions and Pu mobility. Solid PuO_2 phases formed in the presence of mackinawite and chukanovite; however in the case of chukanovite, up to one-third of Pu was also present as Pu(III). For the three investigated reactions of Pu(V) with magnetite, mackinawite, and chukanovite at about pH 8, the concentration of dissolved Fe(II) and the pe values are on the same order of magnitude and thus, by themselves, can only partly account for the different reaction products, suggesting that the Pu redox state distribution found was influenced by the exact type of mineral surfaces present. With respect to Pu surface complexation, it is of relevance that, in contrast to magnetite, mackinawite surfaces are sulfur terminated (Devey et al., 2008), which should considerably reduce their capability to serve as a ligand, as Pu is a hard Lewis acids and therefore oxyphilic(Katz et al., 2006). As these results show in the absence of a surface that allows formation of stable surface complexes, Pu(IV) precipitates as PuO_2. These results also indicated that under reducing conditions, Pu(III) species in addition to PuO_2 needs to be considered for environmental risk assessment, and thermodynamic calculations needed to be supported with spectroscopic data in the study of Pu sorption to mineral surfaces.

Pu sorption studies at environmentally relevant concentrations

The majority of Pu sorption experiments have been performed at concentrations orders of magnitude higher than those observed in the field. For example, actinide concentrations in groundwater samples downgradient of the Mayak and NNSS sites range from 10^{-16}–10^{-12}M, while laboratory experiments are rarely carried out at concentrations <10^{-10}M (Aston and Fowler, 1984; Dai et al., 2005; Geckeis and Rabung, 2008; Keeney-Kennicutt and Morse, 1985; Kersting et al., 1999; Lindahl et al., 2005; Romanchuk et al., 2011). This is particularly problematic for Pu because it is highly insoluble in the +4 oxidation state and can form colloidal particles at concentrations as low as 5 Å~ 10^{-10} M (Neck et al., 2007). Indeed, sorption experiments with both goethite and bentonite clay suggest that precipitation of Pu(IV) at higher concentrations may affect the sorption behavior of

Pu (Missana et al., 2008; Powell et al., 2011). In addition, Snow et al. (2013) demonstrated a concentration dependence for Np(V) sorption to goethite, showing that Kd values differed by an order of magnitude at solution concentrations below 10^{-11} M (equivalent to a Np surface concentration of 10^{-10} mol m^{-2}) compared to higher concentrations(Snow et al., 2013). This suggests that a concentration dependence may exist for Pu even in the absence of precipitation effects (Snow et al., 2013). As a result, sorption predictions using laboratory experiments performed at high concentrations may lead to systematic errors in models of actinide migration in the environment.
Zhao, et al. (2016) investigated Pu(IV) and Pu(V) sorption to goethite over a concentration range of 10^{-15}–10^{-5} M at pH 8. Experiments with initial Pu concentrations of 10^{-15}–10^{-8} M produced linear Pu sorption isotherms, demonstrating that Pu sorption to goethite is not concentration-dependent across this concentration range. Equivalent Pu(IV) and Pu(V) sorption K_d values obtained at 1 and 2-week sampling time points indicated that Pu(V) is rapidly reduced to Pu(IV) on the goethite surface. Further, it suggested that Pu surface redox transformations are sufficiently rapid to achieve an equilibrium state within 1 week, regardless of the initial Pu oxidation state. At initial concentrations >10^{-8} M, both Pu oxidation states exhibited deviations from linear sorption behavior and less Pu was adsorbed than at lower concentrations. NanoSIMS and HRTEM analysis of samples with initial Pu concentrations of 10^{-8}– 10^{-6} M indicated that Pu surface and/or bulk precipitation was likely responsible for this deviation. In 10^{-6}M Pu(IV) and Pu(V) samples, HRTEM analysis showed the formation of a body centered cubic (bcc) Pu_4O_7 structure on the goethite surface, confirming that reduction of Pu(V) had occurred on the mineral surface and that epitaxial distortion previously observed for Pu(IV) sorption occurs with Pu(V) as well.

Pu desorption from mineral surfaces

Desorption of Pu from mineral surfaces has not been as systematically studied as adsorption. Nonetheless, desorption will play a key role in determining the stability of Pu on both immobile and mobile mineral surfaces. Rates of desorption are particularly important as these will control the spatial and temporal extent of Pu migration, especially in colloid-facilitated transport scenarios (Bennett et al., 2017; Saiers and Hornberger, 1996). Pu desorption is typically investigated via batch experiments that have shown that the majority of adsorbed Pu remains associated with the mineral surface, consistent with the high sorption affinity of Pu(IV) for mineral surfaces. For example, Pu(IV) and Pu(V) batch desorption experiments with goethite and hematite have indicated that less than 1% of the solid associated Pu will be desorbed (Lu et al., 1998). Similarly, experiments with sediments from the Esk Estuary, near Sellafield, UK showed that only about 5% of surface-associated Pu(IV) could be desorbed (Hamilton-Taylor et al., 1987). However, greater extents of Pu desorption have been reported for montmorillonite and silica, where up to 20% of Pu was desorbed after a period of 293 days at pH 8.3 (Lu et al., 1998; Lu et al., 2003).

Although both desorption of Pu(IV) and Pu(V) from sediments may occur, the oxidation of Pu(IV) to Pu(V) on the mineral surface appears to be an important mechanism in the

desorption of Pu(IV) (McCubbin and Leonard, 1996; McCubbin et al., 2002). For example, experiments with sediments from Aiken, SC have shown that although adsorbed Pu was present as Pu(IV), desorbed Pu in solution was predominantly Pu(V) (Kaplan et al., 2006). The mobilization of Pu(IV) associated with Irish Sea sediments following exposure to natural sunlight was found to be predominantly Pu(V) thought to be formed via photooxidation of Pu(IV) (McCubbin and Leonard, 1996). The importance of Pu oxidation in its remobilization from mineral surfaces is similar to the behavior of other redox active radionuclides, such as Tc and U, where oxidation of reduced, solid-associated species results in their remobilization (Burke et al., 2006; McBeth et al., 2007; Moon et al., 2007; Newsome et al., 2014).

Begg et al. investigated the role of clay structural Fe on surface mediated reduction reaction by quantifying Pu(V)/(VI) sorption rates under atmospheric (oxic) conditions to three montmorillonite clays with variable Fe content (SWy-1: 2.6 wt % Fe; STx-1: 0.6 wt % Fe; Barasym synthetic mica-montmorillonite: 0.01 wt % Fe) at pH 4, pH 6, and pH 8(Begg et al., 2018). The experiments were performed over a period of one year, a timescale at which the sorption rates were expected to capture both adsorption and surface mediated reduction processes. At pH 6 and pH 8, the rate of sorption was positively correlated with structural Fe content. However, by 360 days, the extent of sorption was independent of Fe. Moreover, in the case of the synthetic montmorillonite it was not apparent that sorption equilibrium had been achieved by the end of the experiment. There was minimal difference in sorption rates between the clays at pH 4, suggesting that structural Fe content may be less important in Pu(V)/(VI) reduction at low pH. The results indicate that at circumneutral pH, structural Fe will affect the kinetics of Pu surface mediated reduction on montmorillonite clays but not necessarily the equilibrium Pu sorption affinity at environmentally relevant timescales. The differences in rates on the three clays emphasize the need to perform long-term sorption experiments (> 1 year) to adequately capture the equilibrium processes controlling the uptake of Pu under atmospheric conditions. Comparison to other minerals indicates that the sorption rates can vary by as much as five orders of magnitude depending on the structure and composition of the surface.

Joseph, et al. (2019) performed flow cell desorption experiments with mineral colloid suspensions produced by hydrothermal alteration of NNSS nuclear melt glass, residual material left behind from nuclear testing. Three different colloid suspensions were used: (1) colloidal material from hydrothermal alteration of nuclear melt glass at 140 °C; (2) at 200 °C; and (3) Pu sorbed to SWy-1 montmorillonite at room temperature. The 140 °C sample contained only montmorillonite, while zeolite and other phases were present in the 200 °C sample. Overall, more Pu was desorbed from the 140 °C colloids (ca. 9−16%) than from the 200 °C colloids (ca. 4−8%). At the end of the flow cell experiments, the desorption rates for the 140 °C colloids and the Pu−montmorillonite colloids were similar while the desorption rates from the 200 °C colloids were up to an order of magnitude lower. The author conclude that the formation of zeolites and clays hydrothermally altered at 200 °C may lead to a more stable association of Pu with colloids, possibly via coprecipitation, resulting in lower desorption rates.

Coprecipitation studies

Pu fate during Fe(III) mineral transformations

Smith et al. (2019) studied the fate of Pu during ferrihydrite to hematite transformation. They demonstrated via EXAFS analysis that under high pH conditions (pH 9), Pu forms an inner-sphere tetradentate complex on the ferrihydrite surface (Smith et al., 2019) which remains unchanged during transformation to hematite, suggesting that Pu remains strongly adsorbed to the iron (oxy)hydroxide surface (Smith et al., 2019) during hematite crystallization.

Balboni et al. (2020) investigated the fate of Pu during the formation of ferrihydrite and its subsequent transformation into goethite. Ferrihydrite was synthesized with varying quantities of Pu(IV) following either a sorption or coprecipitation process; the ferrihydrite was then aged hydrothermally to yield goethite. The synthesized materials were characterized via extended X-ray absorption fine structure spectroscopy, transmission electron microscopy, and acid leaching to elucidate the nature of Pu association with ferrihydrite and goethite. In samples prepared following the sorption method, Pu was identified in two different forms: a PuO_2 precipitate and a surface-sorbed Pu complex. For the samples prepared via coprecipitation, no PuO_2 formation occurs in the ferrihydrite precursor and in the goethite experiments where Pu concentration is <1000 ppm (mg kg(-1)). In these coprecipitation products, EXAFS result indicate Pu is strongly bound to the minerals either via formation of an inner sphere complex, or via an incorporation process. In the coprecipitation experiments, PuO_2 formation only occurs at the highest Pu concentration (3000 ppm), suggesting that during ferrihydrite transformation into goethite, part of the Pu can be remobilized to form PuO_2 nanoparticles. Collectively, our results demonstrate that the nature of Pu associated with the precursor ferrihydrite (adsorbed vs coprecipitated) will have a direct impact on the association of Pu with its alteration product (goethite). Furthermore, the data illustrate that some properties of Pu association with the precursor ferrihydrite are retained through the transformation into goethite. These findings show that Pu strongly associates with iron (oxy)hydroxides formed through coprecipitation processes and in these materials, Pu can be strongly retained by the iron minerals.

Finally Rovnyi et al. (2006) studied the Pu(IV) coprecipitation behavior in solutions containing dibutyl hydrogen phosphate (HDBP) and sodium carbonate. This study was performed to understand the partitioning behavior observed for Np(IV) and Pu(IV/III) in colloidal Fe(III) products during the regeneration organic solvent used in industrial scale spent fuel reprocessing operations. The author speculate that one possible mechanism from Pu removal from solution is the substitution of Pu(III) for Fe(III) in the ferrite like structure FeO. Fe_2O_3, and that colloidal. Pu(IV) products may also be captured by the ferrite structure.

Pu coprecipitation with reduced Fe minerals

Dumas et al. (2019) studied the retention of Pu(V) during coprecipitation with magnetite. After a rapid reduction of Pu(V) to Pu(III) in acidic Fe(II)/Fe(III) solution, base-induced magnetite precipitation ($pH_{exp} \approx 12.5$) leads only to a partial (∼50%) incorporation, while the other half remains at the surface by forming tridentate sorption complexes. Neither solid nor sorbed Pu(IV) species are observed in the starting solution and after precipitation. With Fe(II)-enforced recrystallization at $pH_{exp} = 6.5$, a process potentially mimicking long-term, thermodynamically controlled aging, the equilibrium between both Pu species is even further shifted toward the sorption complex. An analysis of the incorporated species by Pu LIII-edge X ray absorption fine-structure (XAFS) spectroscopy shows a pyrochlore-like coordination environment. In this environment there is a split 8-fold oxygen coordination shell with Pu−O distances of 2.22 and 2.45 Å and an edge-sharing linkage to Fe-octahedra with Pu−Fe distances of 3.68 Å, which is embedded in the magnetite matrix (Pu−Fe distances of 3.93, 5.17, and 5.47 Å). This suggests that the reason for the partial incorporation is the structural incompatibility of the large Pu(III) ion for the octahedral Fe site in magnetite. The adoption of a pyrochlore-like local environment within the magnetite long-range structure might be induced by the rapid coprecipitation rather than being a thermodynamically stable state (kinetic entrapment).

Pu-Fe particles at a contaminated site

Association of Pu with Fe bearing phases has been observed at various contaminated sites. For example in groundwater at the Mayak site (Russia) colloidal amorphous iron oxides with associated Pu were identified (Novikov et al., 2006). Additionally in contaminated soils at Los Alamos National Laboratory, Batuk et al.(2015) identified unusual Pu-Fe particles. The authors suggest that the formation of these particles could have resulted from transitory local chemical conditions from the original waste stream. (Batuk et al., 2015) Finally, Lukashenko et al. (2020) identified particles of Pu containing Fe-Mn oxides in bottom sediments of streams flowing from the tunnels in the Degelen Mountain, a site of the USSR nuclear weapon testing program. Analysis of the particles indicate that these materials may be formed as secondary minerals, suggesting that their formation is most likely related to sorption and coprecipitation of transuranic elements with oxides and hydroxides of iron and manganese (Lukashenko et al., 2020).

4.3 Iodine

Iodine (I) is an electronegative element with relatively large ionic radius. Two isotopes of I are produced during plutonium production: ^{131}I and ^{129}I. ^{131}I has a short half-life of approximately 8 days and quickly decays to ^{131}Xe, as such it is not considered a long-term environmental hazard. ^{129}I is particularly problematic contaminant due to its long half-life (15.7 million years), high yield (0.7% yield per fission of uranium-235) (Nichols and Verpelli, 2007) and weak interactions with common materials in repository environments such as engineering barrier and rock in geology formation (Aimoz et al., 2012; Ojovan and Lee, 2014).

Environmental speciation and redox chemistry

I is characterized by high aqueous solubility, mobility in the environment, and toxicity. In aqueous solution, I can exist in the −1, 0, +1, +3, +5 and +7 oxidation states (Liu and Gunten, 1988). Iodide (I^-) and iodate ($I(V)O_3^-$) are the dominant inorganic species of I found in the environment, whereas elemental I (I_2^0) only exists as a major species at low pH and over a narrow Eh range (Figure 8).

IO_3^- reduction to I^- can occur in sediments (Truex et al., 2017) and while faster in a biotic environment, I reduction also appears to be partially abiotically controlled in acidic conditions (pH < 5) (Grandbois et al., 2018). Therefore, there can be both microbial and abiotic IO_3^--I^- cycling in the subsurface, and only a partially reducing environment is needed to reduce IO_3^-. Iodate (IO_3^-) and iodide (I^-) cannot be degraded or transformed to a less toxic form, and therefore, remedial strategies are required to decrease aqueous concentrations below the drinking water standard (i.e., 1 pCi/L)(Qafoku et al., 2018; Strickland et al., 2017).

The I cycle in the environment is integrally linked with the water cycle. Environmental I movement is dominated by volatilization of organo-I compounds (i.e., iodomethane and others) and I from biological and non-biological sources in the oceans. In fresh water, I primarily occurs as I^- (Whitehead, 1984), and as the salinity or alkalinity of the system is increased, or in the presence of radiation, the I speciation can change to $I(V)O_3^-$ (Whitehead, 1984). Other oxidation states of I may be present in aqueous solutions including the zero-valent, +I and +III oxidation states, although these occur rarely. The I− oxidation is through a two-step process. I− is first transformed to I_2, and then to IO_3^-,with the rate of the transformation being pH dependent and faster under lower pH conditions (Fox et al., 2009). I^- can also be directly oxidized to IO_3^- using a strong oxidizing agent (i.e. peroxide). A comprehensive review of the behavior of I in the environment is given by (Fuge and Johnson, 2015).

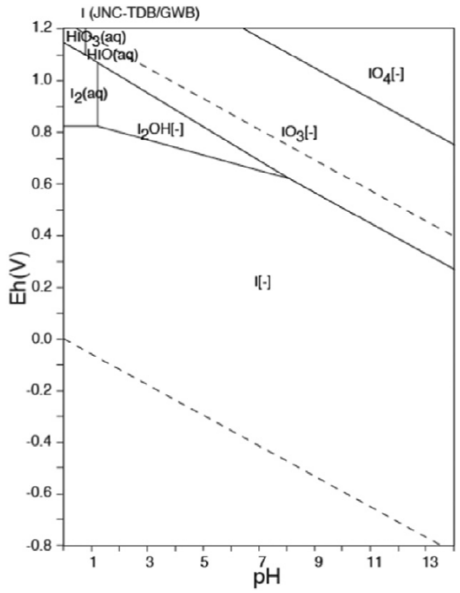

Figure 8 Eh-pH diagram for dominant aqueous species at 25°C from (Moore et al., 2020), calculated considering 10^{-8} mol/L dissolved I. The dashed lines represent the boundaries for the thermodynamic stability of water

Iodine immobilization processes

The mobility of I in the environment is complex and depends on pH, oxidation state, salinity, minerals and microorganisms present in sediment and groundwater. Processes known to affect I mobility include biotic transformations, reactions with sediment-associated iron/manganese, sorption to sediment surfaces, natural organic matter facilitated sorption and accumulation, and co-precipitation with calcium carbonate (Truex et al., 2017). Attenuation mechanisms for I in groundwater include adsorption and interaction with organic matter. Moore et al. (2020) provide a comprehensive review of iodine immobilization processes. In this review we will mostly focus ion discussing I interactions with Fe bearing oxides/minerals.

Iodine adsorption processes with soils and Fe minerals

As previously discussed, the fate and transport of I in the subsurface exhibits complex geochemical behavior, depending upon the chemical speciation, sediment mineral composition, and geochemical conditions. Past studies have demonstrated limited adsorption of IO_3^- and I^- on sediments, especially in a subsurface environment low in organic matter (Kaplan, 2003; Serne et al., 1993) however it was shown that Fe oxides in soils or sediments have a significant impact on I transport (Dai et al., 2004; Dai et al., 2009; Hakimi, 1996; Kaplan, 2003) suggesting that Fe oxides could be good candidates for the subsurface I plume remediation.

Fe oxides and hydroxides are good sorbents of anionic species as a result of the high point of zero charge ($pH_{pzc} > 8$) (Harrison and Berkheiser, 1982; Jain et al., 1999; Li and Kaplan, 2012; Peak and Sparks, 2002; Su and Suarez, 2000; Wang et al., 2001).

Ferrous/ferric iron oxides/(oxy)hydroxides, such as ferrihydrite (Nagata and Fukushi, 2010; Nagata et al., 2009), goethite (FeOOH) (Couture and Seitz, 1983), hematite (Fe_2O_3) (Couture and Seitz, 1983), and magnetite (Fe_3O_4) (Fuhrmann et al., 1998) have potential for I immobilization however they are not selective for I species and will reduce contaminants according to redox potential.

In general, $IO_3^-$is typically adsorbed more strongly than I−, with adsorption inversely related to groundwater pH, especially when they are rich in Fe oxides (Dai et al., 2009), clearly indicating the role of these ubiquitous minerals in controlling I mobility. The behavior of I species toward various Fe oxides and hydroxides is different. This can be explained with the Pearson's Hard Soft Acid Base theory, as IO_3^- is designated as a hard base and I^- is designated as a soft base, and so they are associated with hard and soft acids (i.e., K and Na versus Ag, Cu, and Au), respectively (Cox and Arai, 2014).

Experimental data comparing adsorption extents of I species to different iron oxides and Fe containing minerals/sediments are scarce (Couture and Seitz, 1983; Couture et al., 1979; Kaplan et al., 2000; Machesky et al., 1989; Muramatsu et al., 1990; Nagata and Fukushi, 2010; Nagata et al., 2009; Neal and Truesdale, 1976; Ticknor and Cho, 1990; Whitehead, 1974; Yu et al., 1996). Wang et al. used published data to calculate sorption distribution coefficient (Kd) values for each study as reported in Table 1. A wide range of Kd values [0.6−5640 mL/g] for IO_3^- and non-detectable (ND) to 81.8 mL/g for I^-] were calculated. However, it is difficult to compare these results because experimental conditions and protocols were different. In addition, other important factors, such as the I species transformation via redox reactions (Couture and Seitz, 1983; Hu et al., 2005) and the Fe oxide dissolution at low pH, (Couture and Seitz, 1983) be taken under consideration when evaluating the Kd values reported in Table 1.

sorbent−sorbate	solid/solution ratio (g/L)	initial iodine concentration (ppm)	electrolyte	pH	distribution coefficient, K_d (mL/g)	reference
HFO−iodate	1	126.9	0.1 IS NaCl	4	3878[a]	15
	1	0.04	0.27 M NaCl	8	5640[a]	16
goethite−iodate	10	126.9	0.1 IS NaCl	4	669[a]	15
	10−100	0.018−1.75	5−50% diluted GW[b]	7.7	1.6−25	17
	10	1.2−173.4[c]	0.05 IS	4	207−2857[a]	18
hematite−iodate	100	NA[d]	DDI water	NA[d]	323[a]	19
	10−100	0.018−1.75	5−50% diluted GW	7.7	18−45	17
	310−340	0.33−1.70	0.001 M $NaHCO_3$	6.7−7.0	>99.98%[e]	20
	NA[d]	2×10^{-8}−553	0.1 M CH_3COONa	3.9−8.7	0.6−49	20
	NA[d]	NA[d]	sea water	4.5	37	20
	NA[d]	27−175[c]	DDI	NA[d]	9.6−32.5[a]	21
HFO−iodide	100	63.5	100 mM $NaClO_4$	3.2	11.3[a]	22
	100	63.5	100 mM $NaClO_4$	7.4	0.2[a]	22
	100	6.35−126.9	100 mM $NaClO_4$	5.5	0.9−6.7[a]	22
	1	0.13	0.01 M $NaNO_3$	7	31.6[a]	23
	1	0.04	0.27 M NaCl	8	ND[f]	16
	10	0.1 and 0.4	0.01 M $CaCl_2$	4	45.5−81.8[a]	24
	10	0.1 and 0.4	0.01 M $CaCl_2$	6.5	3.1−6.4[a]	24
goethite−iodide	1	0.13	0.01 M $NaNO_3$	7	3.2[a]	23
	100	0.0006	0.01 M $CaCl_2$	6.1	0.1 ± 0.03	25
	10−100	0.018−1.27	5−50% diluted GW	7.7	ND[f]	17
hematite−iodide	100	NA[d]	DDI water	NA[d]	45.6[a]	19
	10−100	0.013−1.27	5−50% diluted GW	7.7	ND[f]	17
	630	0.013	0.001 M $NaHCO_3$	6.6	0.68[a]	20

[a]Calculated K_d values based on the extracted information in the literature. [b]GW = groundwater. [c]Equilibrium concentrations. [d]NA = not available. [e]IO_3^- removal percentage from aqueous solution. [f]ND = not detectable.

Figure 9 Summary of adsorption studies of IO_3^- and I^- onto Fe oxides as reported from Wang et al,.*(Wang et al., 2019)* References include: *(Couture and Seitz, 1983; Couture et al., 1979; Kaplan et al., 2000; Machesky et al., 1989; Muramatsu et al., 1990; Nagata*

and Fukushi, 2010; Nagata et al., 2009; Neal and Truesdale, 1976; Ticknor and Cho, 1990; Whitehead, 1974; Yu et al., 1996)

Geochemical controls on I species sorption

Overall the IO_3^- or I^- adsorption varies with Fe oxide mineral type, I speciation, solution pH, ionic strength (IS), background solution electrolytes, and the solid/solution ratio. I adsorption to iron oxides is usually pH dependent (Kaplan, 2003; Nagata and Fukushi, 2010; Nagata et al., 2009; Yu et al., 1996). However, in soils that ranged in pH from approximately 4.2 to 8.5, no relationship between IO_3^- adsorption and pH was found, implying a more complex behavior in soils as compared to individual mineral surfaces (i.e., multiple sorbents, surface complexation with uncharged reactive surface groups, etc.) (Dai et al., 2004). There is some evidence that I^- adsorption is more sensitive toward increasing pH than IO_3^-. Kaplan et al. (2003) discovered significantly less I^- was removed from solution when the pH of the soils were above the soil point of zero charge (~pH 4). These results were corroborated in a groundwater characterization study conducted by Li et al. (2013). However, the extent of I^- adsorption may be mineral specific and this may overcome the pH effect (Kennedy et al., 2011). Under laboratory experiments and in near-neutral conditions, hematite (Fe_2O_3) adsorbed all of the IO_3^- and approximately 30% of I^- from solution (Couture and Seitz, 1983). Similar results were found, where greater amounts of IO_3^- were associated with Fe_2O_3 compared to I^-, although both were adsorbed by the Fe oxide (Muramatsu et al., 1990). In a soil column study, positively charged goethite at pH 4.5–6, removed 97% of the IO_3^- (Hakimi, 1996). Ticknor and Cho (1990) looked at adsorption of I^- and IO_3^- to several materials, including hematite and goethite. These experiments were conducted in diluted synthetic groundwater (diluted to 50, 15, and 5%), with a pH of approximately 7.5. I^- adsorption may have been limited due to the pH and ionic strength of the background solution in these experiments. IO_3^- was adsorbed in these same tests, with greater adsorption to hematite than goethite (Ticknor and Cho, 1990). Nagata et al. (Nagata and Fukushi, 2010; Nagata et al., 2009) discovered in experiments conducted with 2-line ferrihydrite and goethite (FeOOH) that, in addition to the effect of pH on both I^- and IO_3^- adsorption extents, increasing ionic strength has a negative impact on I^- adsorption but was negligible for IO_3^- adsorption. This suggests a different mechanism of adsorption for the two species. I^- was adsorbed to 2-line ferrihydrite through outer sphere complexes, while IO_3^- was mostly adsorbed through inner-sphere complexes (Nagata and Fukushi, 2010; Nagata et al., 2009). Fuhrmann et al. (1998) conducted experiments with high concentrations of I and used X-ray absorption spectroscopy to examine IO_3^- and I^- sorption onto a range of Fe-bearing minerals. Magnetite (Fe_3O_4) sorbed I^- from solution but not IO_3^-. In contrast, biotite ($K(Mg,Fe)_3AlSi_3O_{10}(OH,F)_2$) sorbed IO_3^- from solution but did not uptake any I^-. Sorption to either Fe_3O_4 or biotite was not accompanied by any obvious change in speciation, other than a small amount of reduction of I^- to I(0) at the Fe_3O_4 surface (Fuhrmann et al., 1998). Fe_3O_4 and biotite contain Fe(II), and in experiments conducted under the same conditions, but with minerals containing only Fe(III), I sorption did not occur. Thus, the presence of Fe(II) at mineral surfaces is associated with sorption of I. Wang et al. (2019) conducted a series of macroscopic batch experiments to determine the extent of the time-dependent iodate (IO_3^-) and iodide (I^-)

adsorption onto four Fe oxides (i.e., ferrihydrite, goethite, magnetite, and hematite) at different pH values and solution ionic strengths. The results showed that the IO_3^- adsorption extent after 2 days of reacting time followed the order: ferrihydrite (927.5 mL/g) > goethite (84.9 mL/g) > magnetite (23.8 mL/g) > hematite (9.5 mL/g). However, the range of specific surface area normalized Kd values was narrow (2−4.6 mL/m2), suggesting specific surface area controls the adsorption extent. The adsorption extent was correlated negatively with both pH and ionic strength, implying IO_3^- outer-sphere adsorption. The adsorption extent increased or decreased with time (up to ~48%) after 200 days, at relatively high or low I concentration ranges, respectively, likely because of multiple geochemical reactions, including interparticle diffusion, mineral transformation, and I speciation changes. I− adsorption was insignificant for all Fe oxides.

Interactions with organic matter and microorganisms

Microorganisms can catalyze I oxidation, reduction, accumulation, volatilization, and enhance incorporation into organic matter (Kaplan et al., 2014). Organo-I may play a role in I precipitation and sorption processes. I is often associated with organic matter in soils, but studies have shown that while I^- has a strong association with organic matter, especially at pH <6 (Dai et al., 2009; Kaplan, 2003; Muramatsu et al., 1990), IO_3^- association with organic matter is not as clear. Some studies suggest that IO_3^- is not strongly associated with the organic matter (Dai et al., 2009; Kaplan, 2003; Muramatsu et al., 1990), while others have differing results (Li et al., 2017; Xu et al., 2015; Zhang et al., 2011). For example at DOE sites, the presence of organic material has a strong effect on total I retention in Savannah River Site (Emerson et al., 2014; Schwehr et al., 2009) soils and some of the I at the Hanford Site is associated with organic matter (Qafoku et al., 2018; Truex et al., 2017).

Other immobilization processes and materials

For a comprehensive review of immobilization iodine immobilization processes including coprecipitation or encapsulation via calcite, apatite, metal substituted apatite, sulfur-, silver-, cupper- and bismuth-based materials, metal organic frameworks, layered double hydroxides and aerogels refer to (Moore et al., 2020). In our literature search we did not find any study in the literature that addresses the fate of I during coprecipitation reactions with Fe minerals.

5. Interpreting coprecipitation data by calculating partitioning coefficients in coprecipitation reactions

The Doerner-Hoskins (1925) relationship is often invoked to parameterize the processes of sorption and coprecipitation of a trace element within a mineral matrix. It is based on the relationship between the trace metal and major element in solution and on the surface of a precipitating phase such that:

$$\lambda_{Me} = \frac{X_{Me}}{X_{Fe}} \times \frac{[Fe]}{[Me]} \quad (1)$$

where X refers to the mol fraction of the trace metal or major element on the surface and the [Fe] and [Me] refer to the aqueous concentration of the trace metal and major element in solution. For a closed system coprecipitation experiment, the logarithmic law can be used to determine l from the initial and final concentrations of the major and trace element during a coprecipitation reaction such that:

$$ln\left(\frac{[Me]}{[Me]_0}\right) = \lambda_{Me} ln\left(\frac{[Fe]}{[Fe]_0}\right) \quad (2)$$

Where $[Me]_0$ and $[Fe]_0$ refer to the initial aqueous concentration of the trace metal and major element, respectively and [Me] and [Fe] are the aqueous concentration of the trace metal and major element during the coprecipitation experiment. The λ values in equations 1 and 2 are defined by Curti (1999) as phenomenological in that the relationship is based on the total concentration of major element and trace metal. The relationship does not account for effects such as pH, ionic strength, fluid composition that may affect the partitioning of the trace metal into the precipitate. Using equation 2 we calculated concentration of trace metal and Fe during precipitation at three different values of λ_{Me} (Figure 10).

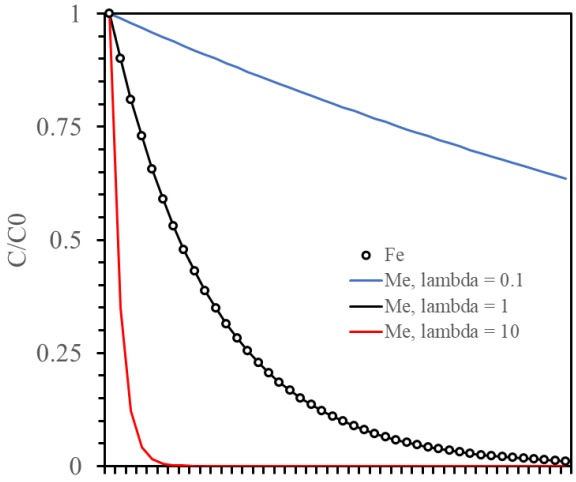

Figure 10 Concentration of trace metal and Fe during precipitation at three different values of lambda based on Equation 2.

We calculated λ_{Me} using data from literature that describe coprecipitation of Tc, Se, Np and Pu in a suite of Fe(II), Fe(II/III) and Fe(III) minerals (please note reference for Tc and Se were reported in last year progress report). In Figure 11 the values of lambda (on x axis) are compared to % of radionuclide uptake, which represents how much radionuclide is sequestered by a mineral phase after mineral precipitation. Our results show that overall, the calculated λ_{Me}values increase as the % of coprecipitation increases. For solids that retain <70% radionuclides lambda in usually <0.1, which is close to what we expected based on Figure 10.

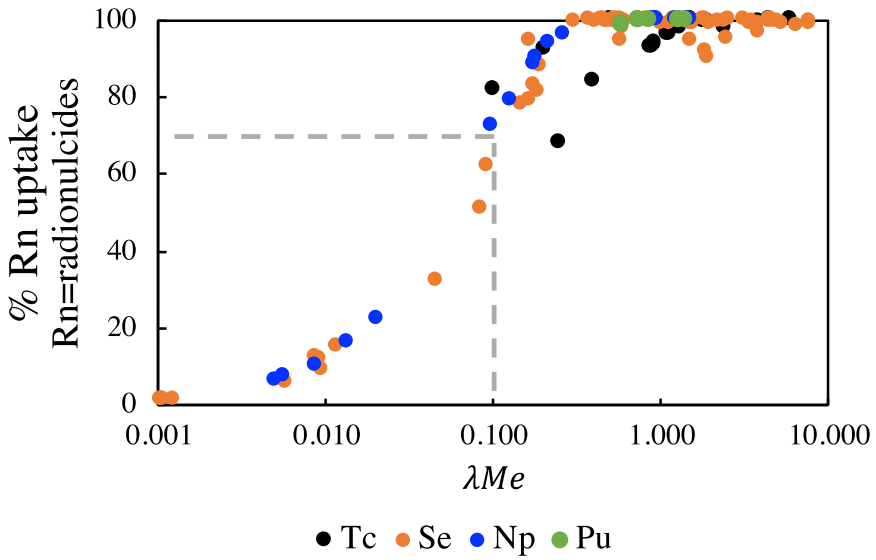

Figure 11 $\lambda_{\text{Me calculated for coprecipitation}}$ reaction of Tc, Se, Np and Pu with Fe minerals

The Se example

Amongst the radionuclides considered in this study, the Se literature is the most comprehensive in addressing Se coprecipitation behavior with Fe minerals, and the calculated λ_{Me} span the largest range (0.001-8). Borsig et al. (Borsig et al., 2018; Börsig et al., 2017) and Diener et al. (Diener and Neumann, 2011; Diener et al., 2012) provide comprehensive data set of Se (VI, IV, -II) coprecipitation with various Fe oxide minerals including Fe(III), mixed Fe(II/III) and Fe sulfides and their data set were analyzed to determine trends in the calculated λ_{Me} values.

The lowest values of λ_{Me} are observed for Se(VI) coprecipitation with Fe(III) minerals. The λ_{Me} values increase slightly for coprecipitation of Se(VI) with reduced Fe minerals and became higher for Se(IV) coprecipitated with mixed Fe(II/III) minerals. The highest λ_{Me} values are measured for reduced selenium (-II) in coprecipitation reaction with reduced Fe minerals, such as pyrite. This general trend seems to be consistent with Se geochemical behaviour observed in sorption reactions.

Although a few assumptions need to be made to calculate λ_{Me} (specifically regarding the $[Fe_0]$ concentration) we conclude that λ_{Me} provides a valid approach to describe radionuclide coprecipitation behavior with Fe minerals from data sourced from the literature.

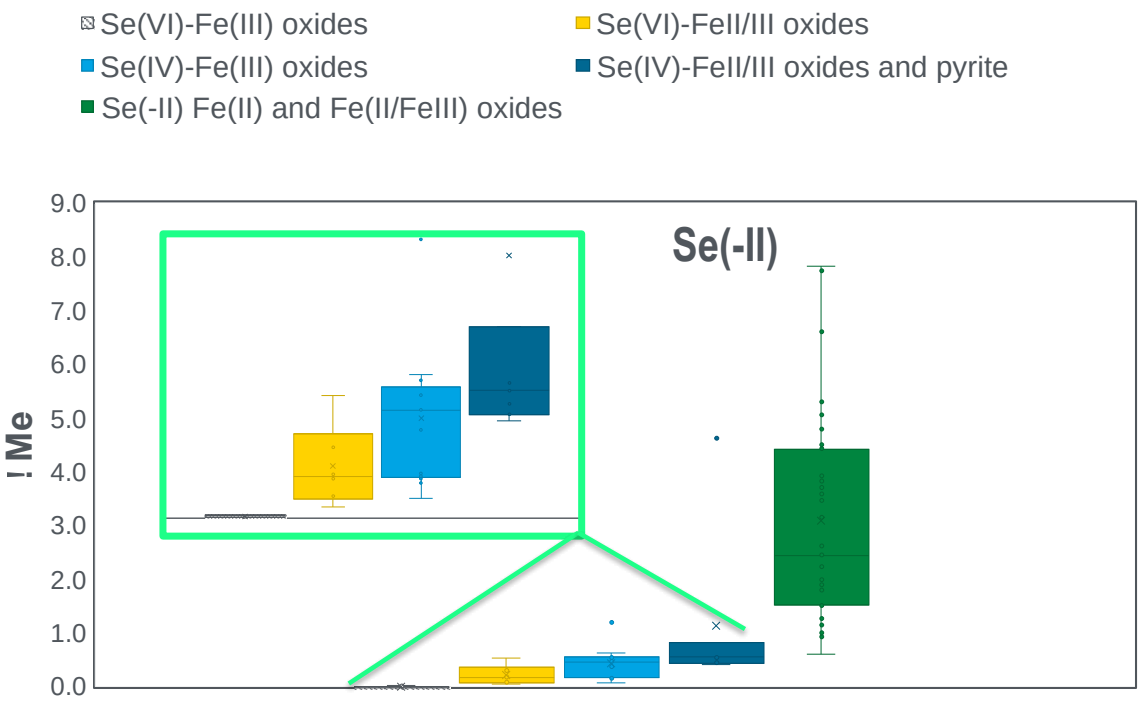

Figure 12 λ_{Me} values calculated for Se coprecipitation reactions with Fe minerals

6. FY22 Efforts

Our FY22 effort will focus on completing our analysis of radionuclide incorporation into Fe oxide phases and evaluation of λ_{Me} values across a range of radionuclides relevant to performance assessment models. Based on our assessment of the relevance of this process in radionuclide retention and sequestration in corrosion products, we plan to initiate focused corrosion and coprecipitation experiments to that will address the limitations of data available in the literature. For example, no data are available for the incorporation of I into corrosion products. As a result, we are not able to assess its potential impact on I migration from repository near fields. The scope of experiments will be determined in consultation with SFWST and the needs of the program and GDSA.

7. Acknowledgments

This work was supported by the Spent Fuel and Waste Science and Technology campaign of the Department of Energy's Nuclear Energy Program. Prepared by LLNL under Contract DE-AC52-07NA27344.

8. References

Aimoz, L., Wieland, E., Taviot-Guého, C., Dähn, R., Vespa, M. and Churakov, S.V. (2012) Structural Insight into Iodide Uptake by AFm Phases. Environmental Science & Technology 46, 3874-3881.

Alessi, D.S., Szymanowski, J.E.S., Forbes, T.Z., Quicksall, A.N., Sigmon, G.E., Burns, P.C. and Fein, J.B. (2013) Mineralogic controls on aqueous neptunium(V) concentrations in silicate systems. Journal of Nuclear Materials 433, 233-239.

Allen, P.G., Bucher, J.J., Shuh, D.K., Edelstein, N.M. and Reich, T. (1997) Investigation of Aquo and Chloro Complexes of UO22+, NpO2+, Np4+, and Pu3+ by X-ray Absorption Fine Structure Spectroscopy. Inorganic Chemistry 36, 4676-4683.

Antonio, M.R., Soderholm, L., Williams, C.W., Blaudeau, J.P. and Bursten, B.E. (2001) Neptunium redox speciation. Radiochim Acta 89, 17-25.

Arai, Y., Moran, P.B., Honeyman, B.D. and Davis, J.A. (2007) In situ spectroscopic evidence for neptunium(V)-carbonate inner-sphere and outer-sphere ternary surface complexes on hematite surfaces. Environmental Science & Technology 41, 3940-3944.

Artinger, R., Marquardt, C.M., Kim, J.I., Seibert, A., Trautmann, N. and Kratz, J.V. (2000) Humic colloid-borne Np migration: influence of the oxidation state. Radiochimica Acta 88, 609-612.

Aston, S.R. and Fowler, S.W. (1984) Experimental Studies on the Bioaccumulation of Plutonium from Sea-Water and a Deep-Sea Sediment by Clams and Polychaetes. Journal of Environmental Radioactivity 1, 67-78.

Bach, D., Christiansen, B., Schild, D. and Geckeis, H. (2014) TEM study of Green Rust Sodium Sulphate (GRNa,SO4) Interacted with Neptunyl Ions (NpO2+). Radiochimica Acta 102, 279-289.

Balboni, E., Morrison, J.M., Wang, Z., Engelhard, M.H. and Burns, P.C. (2015) Incorporation of Np(V) and U(VI) in carbonate and sulfate minerals crystallized from aqueous solution. Geochimica et Cosmochimica Acta 151, 133-149.

Balboni, E., Smith, K.F., Moreau, L.M., Li, T.T., Maloubier, M., Booth, C.H., Kersting, A.B. and Zavarin, M. (2020) Transformation of Ferrihydrite to Goethite and the Fate of Plutonium. Acs Earth and Space Chemistry 4, 1993-2006.

Banik, N.L., Buda, R.A., Burger, S., Kratz, J.V. and Trautmann, N. (2007) Sorption of tetravalent plutonium and humic substances onto kaolinite. Radiochimica Acta 95, 569-575.

Batuk, O.N., Conradson, S.D., Aleksandrova, O.N., Boukhalfa, H., Burakov, B.E., Clark, D.L., Czerwinski, K.R., Felmy, A.R., Lezama-Pacheco, J.S., Kalmykov, S.N., Moore, D.A., Myasoedov, B.F., Reed, D.T., Reilly, D.D., Roback, R.C., Vlasova, I.E., Webb, S.M. and Wilkerson, M.P. (2015) Multiscale Speciation of U and Pu at Chernobyl, Hanford, Los Alamos, McGuire AFB, Mayak, and Rocky Flats. Environmental Science & Technology 49, 6474-6484.

Baumer, T. and Hixon, A.E. (2019) Kinetics of neptunium sorption and desorption in the presence of aluminum (hydr)oxide minerals: Evidence for multi-step desorption at low pH. Journal of Environmental Radioactivity 205, 72-78.

Baumer, T., Kay, P. and Hixon, A.E. (2017) Comparison of europium and neptunium adsorption to aluminum (hydr)oxide minerals. Chemical Geology 464, 84-90.

Begg, J.D., Edelman, C., Zavarin, M. and Kersting, A.B. (2018) Sorption kinetics of plutonium (V)/(VI) to three montmorillonite clays. Applied Geochemistry 96, 131-137.

Begg, J.D., Zavarin, M. and Kersting, A.B. (2017) Desorption of plutonium from montmorillonite: An experimental and modeling study. Geochimica Et Cosmochimica Acta 197, 278-293.

Begg, J.D., Zavarin, M., Tumey, S.J. and Kersting, A.B. (2015) Plutonium sorption and desorption behavior on bentonite. Journal of Environmental Radioactivity 141, 106-114.

Begg, J.D., Zavarin, M., Zhao, P., Tumey, S.J., Powell, B. and Kersting, A.B. (2013) Pu(V) and Pu(IV) sorption to montmorillonite. Environmental Science & Technology 47, 5146-5153.

Bennett, J.W., Bjorklund, J.L., Forbes, T.Z. and Mason, S.E. (2017) Systematic Study of Aluminum Nanoclusters and Anion Adsorbates. Inorganic Chemistry 56, 13014-13028.

Borsig, N., Scheinost, A.C., Shaw, S., Schild, D. and Neumann, T. (2018) Retention and multiphase transformation of selenium oxyanions during the formation of magnetite via iron(II) hydroxide and green rust. Dalton Transactions 47, 11002-11015.

Börsig, N., Scheinost, A.C., Shaw, S., Schild, D. and Neumann, T. (2017) Uptake mechanisms of selenium oxyanions during the ferrihydrite-hematite recrystallization. Geochimica et Cosmochimica Acta 206, 236-253.

Bots, P., Shaw, S., Law, G.T.W., Marshall, T.A., Mosselmans, J.F.W. and Morris, K. (2016) Controls on the Fate and Speciation of Np(V) During Iron (Oxyhydr)oxide Crystallization. Environmental Science & Technology 50, 3382-3390.

Bradbury, M.H. and Baeyens, B. (2006) Modelling sorption data for the actinides Am(III), Np(V) and Pa(V) on montmorillonite. Radiochimica Acta 94, 619-625.

Bruno, J. and Ewing, R.C. (2006) Spent nuclear fuel. Elements 2, 343-349.

Burke, I.T., Boothman, C., Lloyd, J.R., Livens, F.R., Charnock, J.M., McBeth, J.M., Mortimer, R.J.G. and Morris, K. (2006) Reoxidation behavior of technetium, iron, and sulfur in estuarine sediments. Environmental Science & Technology 40, 3529-3535.

Burns, P.C., Deely, K.M. and Skanthakumar, S. (2004) Neptunium incorporation into uranyl compounds that form as alteration products of spent nuclear fuel: Implications for geologic repository performance. Radiochimica Acta 92, 151-159.

Burns, P.C., Ewing, R.C. and Navrotsky, A. (2012) Nuclear Fuel in a Reactor Accident. Science 335, 1184-1188.

Burns, P.C. and Klingensmith, A.L. (2006) Uranium mineralogy and neptunium mobility. Elements 2, 351-356.

Cantrell, K.J. (2009) Transuranic Contamination in Sediment and Groundwater at the U.S. DOE Hanford Site. ; Pacific Northwest National Lab. (PNNL), Richland, WA (United States), p. Medium: ED; Size: PDFN.

Cantrell, K.J., Um, W., Williams, B.D., Bowden, M.E., Gartman, B., Lukens, W.W., Buck, E.C. and Mausolf, E.J. (2014) Chemical stabilization of Hanford tank residual waste. Journal of Nuclear Materials 446, 246-256.

Chatterjee, S., Bryan, S.A., Casella, A.J., Peterson, J.M. and Levitskaia, T.G. (2017) Mechanisms of neptunium redox reactions in nitric acid solutions. Inorg Chem Front 4, 581-594.

Choppin, G.R. (1983) Solution Chemistry of the Actinides. Radiochimica Acta 32, 43-53.

Choppin, G.R. (1991) Redox speciation of plutonium in natural waters. J Radioan Nucl Ch Ar 147, 109-116.

Christiansen, B.C., Geckeis, H., Marquardt, C.M., Bauer, A., Römer, J., Wiss, T., Schild, D. and Stipp, S.L.S. (2011) Neptunyl (NpO2+) interaction with green rust, GRNa,SO4. Geochimica et Cosmochimica Acta 75, 1216-1226.

Clark, D.L., Hobart, D.E. and Neu, M.P. (1995) Actinide Carbonate Complexes and their Importance in Actinide Environmental Chemistry. Chemical reviews 95, 25-48.

Cohen, D. and Hindman, J.C. (1952) The Neptunium(Iv) Neptunium(V) Couple in Perchloric Acid - the Partial Molal Heats and Free Energies of Formation of Neptunium Ions. Journal of the American Chemical Society 74, 4682-4685.

Combes, J.M., Chisholm-Brause, C.J., Brown G E, J.R., Parks, G.A., Conradson, S.D., Eller, P.G., Triay, I.R., Hobart, D.E. and Meijer, A. (1992) EXAFS spectroscopic study of neptunium(V) sorption at the goethite/water interface. Environmental Science and Technology 26, 376-382.

Conradson, S.D., Abney, K.D., Begg, B.D., Brady, E.D., Clark, D.L., den Auwer, C., Ding, M., Dorhout, P.K., Espinosa-Faller, F.J., Gordon, P.L., Haire, R.G., Hess, N.J., Hess, R.F., Keogh, D.W., Lander, G.H., Lupinetti, A.J., Morales, L.A., Neu, M.P., Palmer, P.D., Paviet-Hartmann, P., Reilly, S.D., Runde, W.H., Tait, C.D., Veirs, D.K. and Wastin, F. (2004) Higher order speciation effects on plutonium L-3 X-ray absorption near edge spectra. Inorganic Chemistry 43, 116-131.

Couture, R.A. and Seitz, M.G. (1983) Sorption of Anions of Iodine by Iron-Oxides and Kaolinite. Nuclear and Chemical Waste Management 4, 301-306.

Couture, R.A., Seitz, M.G. and Steindler, M.J. (1979) Adsorption of Iodate by Hematite (Fe2o3). T Am Nucl Soc 32, 397-397.

Cox, E.M. and Arai, Y. (2014) Chapter Two - Environmental Chemistry and Toxicology of Iodine, in: Sparks, D.L. (Ed.), Advances in Agronomy. Academic Press, pp. 47-96.

Curti, E. (1999) Coprecipitation of radionuclides with calcite: estimation of partition coefficients based on a review of laboratory investigations and geochemical data. Applied Geochemistry 14, 433-445.

Dai, J.-L., Zhang, M. and Zhu, Y.-G. (2004) Adsorption and desorption of iodine by various Chinese soils: I. Iodate. Environment International 30, 525-530.

Dai, J.L., Zhang, M., Hu, Q.H., Huang, Y.Z., Wang, R.Q. and Zhu, Y.G. (2009) Adsorption and desorption of iodine by various Chinese soils: II. Iodide and iodate. Geoderma 153, 130-135.

Dai, M.H., Buesseler, K. and Pike, S.M. (2005) Plutonium in groundwater at the 100K-Area of the US DOE Hanford site. Journal of Contaminant Hydrology 76, 167-189.

Dalodiere, E., Virot, M., Dumas, T., Guillaumont, D., Illy, M.C., Berthon, C., Guerin, L., Rossberg, A., Venault, L., Moisy, P. and Nikitenko, S.I. (2018) Structural and magnetic susceptibility characterization of Pu(V) aqua ion using sonochemistry as a facile synthesis method. Inorg Chem Front 5, 100-111.

Dalodiere, E., Virot, M., Morosini, V., Chave, T., Dumas, T., Hennig, C., Wiss, T., Blanco, O.D., Shuh, D.K., Tyliszcak, T., Venault, L., Moisy, P. and Nikitenko, S.I. (2017) Insights into the sonochemical synthesis and properties of salt-free intrinsic plutonium colloids. Sci Rep-Uk 7.

Del Nero, M., Ben Said, K., Made, B., Clement, A. and Bontems, G. (1998) Effect of pH and carbonate concentration in solution on the sorption of neptunium(V) by hydrargilite: Application of the non-electrostatic model. Radiochimica Acta 81, 133-141.

Devey, A.J., Grau-Crespo, R. and de Leeuw, N.H. (2008) Combined density functional theory and interatomic potential study of the bulk and surface structures and properties of the iron sulfide mackinawite (FeS). Journal of Physical Chemistry C 112, 10960-10967.

Di Giandomenico, M.V., Le Naour, C., Simoni, E., Guillaumont, D., Moisy, P., Hennig, C., Conradson, S.D. and Den Auwer, C. (2009) Structure of early actinides(V) in acidic solutions. Radiochimica Acta 97, 347-353.

Diener, A. and Neumann, T. (2011) Synthesis and incorporation of selenide in pyrite and mackinawite. Radiochimica Acta 99, 791-798.

Diener, A., Neumann, T., Kramar, U. and Schild, D. (2012) Structure of selenium incorporated in pyrite and mackinawite as determined by XAFS analyses. Journal of Contaminant Hydrology 133, 30-39.

Downward, L., Booth, C.H., Lukens, W.W. and Bridges, F. (2007) A variation of the F-Test for determining statistical relevance of particular parameters in EXAFS fits. Aip Conf Proc 882, 129-+.

Dumas, T., Fellhauer, D., Schild, D., Gaona, X., Altmaier, M. and Scheinost, A.C. (2019) Plutonium Retention Mechanisms by Magnetite under Anoxic Conditions: Entrapment versus Sorption. Acs Earth and Space Chemistry 3, 2197-2206.

Efurd, D.W., Runde, W., Banar, J., Janecky, D., Kaszuba, J., Palmer, P., Roensch, F. and Tait, C.D. (1998) Neptunium and Plutonium Solubilities in a Yucca Mountain Groundwater. Environmental science technology 32, 3893-3900.

Emerson, H.P., Xu, C., Ho, Y.F., Zhang, S., Schwehr, K.A., Lilley, M., Kaplan, D.I., Santschi, P.H. and Powell, B.A. (2014) Geochemical controls of iodine uptake and transport in Savannah River Site subsurface sediments. Applied Geochemistry 45, 105-113.

Fernelius, W.C. and Detling, K.D. (1934) Preparation of crystals of sparingly soluble salts. Journal of chemical education 11, 176.

Finch, R.J., Buck, E.C., Finn, P.A. and Bates, J.K. (1999) Oxidative corrosion of spent UO2 fuel in vapor and dripping groundwater at 90 degrees C. MATERIALS RESEARCH SOCIETY, WARRENDALE, pp. 431-438.

Forbes, T.Z. and Burns, P.C. (2006) Ba(NpO2)(PO4)(H2O), its relationship to the uranophane group, and implications for Np incorporation in uranyl minerals. American Mineralogist 91, 1089-1093.

Forbes, T.Z., Wallace, C. and Burns, P.C. (2008) Neptunyl Compounds: Polyhedron Geometries, Bond-Valence Parameters, and Structural Hierarchy. Canadian Mineralogist 46, 1623-1645.

Fox, P.M., Davis, J.A. and Luther, G.W. (2009) The kinetics of iodide oxidation by the manganese oxide mineral birnessite. Geochimica Et Cosmochimica Acta 73, 2850-2861.

Fuge, R. and Johnson, C.C. (2015) Iodine and human health, the role of environmental geochemistry and diet, a review. Applied Geochemistry 63, 282-302.

Fuhrmann, M., Bajt, S. and Schoonen, M.A.A. (1998) Sorption of iodine on minerals investigated by X-ray absorption near edge structure (XANES) and I-125 tracer sorption experiments. Applied Geochemistry 13, 127-141.

Geckeis, H. and Rabung, T. (2008) Actinide geochemistry: From the molecular level to the real system. Journal of Contaminant Hydrology 102, 187-195.

Geckeis, H., Zavarin, M., Salbu, B., Lind, O.C. and Skipperud, L. (2019) Environmental chemistry of Plutonium, Plutonium Handbook, 2nd ed. American Nuclear Society.

Gerber, E., Romanchuk, A.Y., Pidchenko, I., Amidani, L., Rossberg, A., Hennig, C., Vaughan, G.B.M., Trigub, A., Egorova, T., Bauters, S., Plakhova, T., Hunault, M.O.J.Y., Weiss, S., Butorin, S.M., Scheinost, A.C., Kalmykov, S.N. and Kvashnina, K.O. (2020) The missing pieces of the PuO2 nanoparticle puzzle. Nanoscale.

Girvin, D.C., Ames, L.L., Schwab, A.P. and McGarrah, J.E. (1991) Neptunium adsorption on synthetic amorphous Iron oxyhydroxide. Journal of Colloid and Interface Science 141, 67-78.

Grandbois, R., Yeager, C., Tani, Y., Xu, C., Zhang, S.J., Beaver, M., Schwehr, K., Kaplan, D. and Santschi, P. (2018) Biogenic Manganese Oxides Facilitate Iodide Oxidation at pH <= 5. Geomicrobiology Journal 35, 167-173.

Guckel, K., Rossberg, A., Muller, K., Brendler, V., Bernhard, G. and Foerstendorf, H. (2013) Spectroscopic Identification of Binary and Ternary Surface Complexes of Np(V) on Gibbsite. Environmental Science & Technology 47, 14418-14425.

Hakanen, M. and Lindberg, A. (1991) Sorption of Neptunium under Oxidizing and Reducing Groundwater Conditions. Radiochimica Acta 52-3, 147-151.

Hakimi, S.S. (1996) Improved iodine-125 removal in anionic form of iodate by column method using laterite soil. Journal of Radioanalytical and Nuclear Chemistry 214, 117-131.

Hamilton-Taylor, J., Kelly, M., Mudge, S. and Bradshaw, K. (1987) Rapid remobilization of plutonium from estuarine sediments. Journal of Environmental Radioactivity 5, 409-423.

Harrison, J.B. and Berkheiser, V.E. (1982) Anion Interactions with Freshly Prepared Hydrous Iron Oxides. Clay Clay Min. 30, 97-102.

Heberling, F., Denecke, M.A. and Bosbach, D. (2008) Neptunium(V) coprecipitation with calcite. Environmental science & technology 42, 471-476.

Heberling, F., Scheinost, A.C. and Bosbach, D. (2011) Formation of a ternary neptunyl(V) biscarbonato inner-sphere sorption complex inhibits calcite growth rate. Journal of contaminant hydrology 124, 50-56.

Hennig, C., Ikeda Ohno, A., Tsushima, S. and Scheinost, A. (2009) The sulfate coordination of Np(IV), Np(V), and Np(VI) in aqueous solution. Inorganic chemistry 48, 5350-5360.

Hixon, A.E., Hu, Y.J., Kaplan, D.I., Kukkadapu, R.K., Nitsche, H., Qafoku, O. and Powell, B.A. (2010) Influence of iron redox transformations on plutonium sorption to sediments. Radiochimica Acta 98, 685-692.

Hixon, A.E. and Powell, B.A. (2018) Plutonium environmental chemistry: mechanisms for the surface-mediated reduction of Pu(v/vi). Environ Sci-Proc Imp 20, 1306-1322.

Hu, Q.H., Zhao, P.H., Moran, J.E. and Seaman, J.C. (2005) Sorption and transport of iodine species in sediments from the Savannah River and Hanford Sites. Journal of Contaminant Hydrology 78, 185-205.

Hu, Y.-J., Kestrel Schwaiger, L., Booth Corwin, H., Kukkadapu Ravi, K., Cristiano, E., Kaplan, D. and Nitsche, H. (2010) Molecular interactions of plutonium(VI) with synthetic manganese-substituted goethite, Radiochimica Acta International journal for chemical aspects of nuclear science and technology, p. 655.

Husar, R., Weiss, S., Hennig, C., Hubner, R., Ikeda-Ohno, A. and Zanker, H. (2015) Formation of Neptunium(IV)-Silica Colloids at Near-Neutral and Slightly Alkaline pH. Environmental Science & Technology 49, 665-671.

Icopini, G.A., Lack, J.G., Hersman, L.E., Neu, M.P. and Boukhalfa, H. (2009) Plutonium(V/VI) reduction by the metal-reducing Bacteria Geobacter metallireducens GS-15 and Shewanella oneidensis MR-1. Appl Environ Microb 75, 3641-3647.

Ikeda-Ohno, A., Hennig, C., Rossberg, A., Funke, H., Scheinost, A.C., Bernhard, G. and Yaita, T. (2008) Electrochemical and complexation behavior of neptunium in aqueous perchlorate and nitrate solutions. Inorganic Chemistry 47, 8294-8305.

Jain, A., Raven, K.P. and Loeppert, R.H. (1999) Arsenite and Arsenate Adsorption on Ferrihydrite: Surface Charge Reduction and Net OH- Release Stoichiometry. Environmental Science & Technology 33, 1179-1184.

Jain, A., Rawat, N., Kumar, S., Tomar, B.S., Manchanda, V.K. and Ramanathan, S. (2007) Effect of humic acid on sorption of neptunium on hematite colloids. Radiochimica Acta 95, 501-506.

Joseph, C., Balboni, E., Baumer, T., Treinen, K., Kersting, A.B. and Zavarin, M. (2019) Plutonium Desorption from Nuclear Melt Glass-Derived Colloids and Implications for Migration at the Nevada National Security Site, USA. Environmental Science & Technology 53, 12238-12246.

Kalmykov, S.N., Schafer, T., Claret, F., Perminova, I.V., Petrova, A.B., Shcherbina, N.S. and Teterin, Y.A. (2008) Sorption of neptunium onto goethite in the presence of humic acids with different hydroquinone group content. Radiochimica Acta 96, 685-690.

Kaplan, D.I. (2003) Influence of surface charge of an Fe-oxide and an organic matter dominated soil on iodide and pertechnetate sorption. Radiochimica Acta 91, 173-178.

Kaplan, D.I., Denham, M.E., Zhang, S., Yeager, C., Xu, C., Schwehr, K.A., Li, H.P., Ho, Y.F., Wellman, D. and Santschi, P.H. (2014) Radioiodine Biogeochemistry and Prevalence in Groundwater. Crit Rev Env Sci Tec 44, 2287-2335.

Kaplan, D.I., Powell, B.A., Gumapas, L., Coates, J.T., Fjeld, R.A. and Diprete, D.P. (2006) Influence of pH on plutonium desorption/solubilization from sediment. Environmental Science & Technology 40, 5937-5942.

Kaplan, D.I., Serne, R.J., Parker, K.E. and Kutnyakov, I.V. (2000) Iodide sorption to subsurface sediments and illitic minerals. Environmental Science & Technology 34, 399-405.

Kaszuba, J.P. and Runde, W.H. (1999) The aqueous geochemistry of neptunium: Dynamic control of soluble concentrations with applications to nuclear waste disposal. Environmental science {\&} technology 33, 4427-4433.

Katz, J.J., Morss, L.R., Edelstein, N.M. and Fuger, J. (2006) The chemistry of the actinide and transactinide elements, in: Morss, L.R., Edelstein, N.M., Fuger, J. (Eds.), The Chemistry of the Actinide and Transactinide Elements. Springer Netherlands, pp. 1-17.

Katz, L.E. and Hayes, K.F. (1995) J. Colloid Interface Sci. 170, 477.

Keeney-Kennicutt, W.L. and Morse, J.W. (1985) The redox chemistry of $Pu(V)O_2^+$ interaction with common mineral surfaces in dilute solutions and seawater. Geochimica Et Cosmochimica Acta 49, 2577-2588.

Kelly, S.D., Rasbury, E.T., Chattopadhyay, S., Kropf, A.J. and Kemner, K.M. (2006) Evidence of a stable uranyl site in ancient organic-rich calcite. Environmental Science Technology 40, 2262-2268.

Kennedy, C.B., Gault, A.G., Fortin, D., Clark, I.D. and Ferris, F.G. (2011) Retention of Iodide by Bacteriogenic Iron Oxides. Geomicrobiology Journal 28, 387-395.

Kersting, A.B., Efurd, D.W., Finnegan, D.L., Rokop, D.J., Smith, D.K. and Thompson, J.L. (1999) Migration of plutonium in ground water at the Nevada Test Site. Nature 397, 56-59.

Kersting, A.B., Reimus, P.W., Abdel-Fattah, A., Allen, P.G., Anghel, I., Benedict, F.C., Esser, B.K., Lu, N., Kung, K.S., Nelson, J., Neu, M.P., Reilly, S.D., Smith, D.K., Sylwester, E.R., Wang, L., Ware, S.D., Warren, R., Williams, R.W., Zavarin, M. and Zhao, P. (2003) Colloid-Facilitated Transport of Low-Solubility Radionuclides: A Field, Experimental, and Modeling Investigation. ; Lawrence Livermore National Lab. (LLNL), Livermore, CA (United States), pp. Medium: ED; Size: PDF-file: 285 pages; size: 210.283 Mbytes.

Khasanova, A.B., Kalmykov, S.N., Perminova, I.V. and Clark, S.B. (2007) Neptunium redox behavior and sorption onto goethite and hematite in the presence of humic acids with different hydroquinone content. Journal of Alloys and Compounds 444, 491-494.

Kirsch, R., Fellhauer, D., Altmaier, M., Neck, V., Rossberg, A., Fanghanel, T., Charlet, L. and Scheinost, A.C. (2011) Oxidation State and Local Structure of Plutonium Reacted with Magnetite, Mackinawite, and Chukanovite. Environmental Science & Technology 45, 7267-7274.

Klingensmith, A.L. and Burns, P.C. (2007) Neptunium substitution in synthetic uranophane and soddyite. American Mineralogist 92, 1946-1951.

Kohler, M., Honeyman, B.D. and Leckie, J.O. (1999) Neptunium(V) sorption on hematite (alpha-Fe2O3) in aqueous suspension: The effect of CO2. Radiochimica Acta 85, 33-48.

Kvashnina, K.O., Romanchuk, A.Y., Pidchenko, I., Amidani, L., Gerber, E., Trigub, A., Rossberg, A., Weiss, S., Popa, K., Walter, O., Caciuffo, R., Scheinost, A.C., Butorin, S.M. and Kalmykov, S.N. (2019) A Novel Metastable Pentavalent Plutonium Solid Phase on the Pathway from Aqueous Plutonium(VI) to PuO2 Nanoparticles. Angewandte Chemie-International Edition 58, 17558-17562.

Li, D. and Kaplan, D.I. (2012) Sorption coefficients and molecular mechanisms of Pu, U, Np, Am and Tc to Fe (hydr)oxides: A review. Journal of Hazardous Materials 243, 1-18.

Li, J.X., Wang, Y.X., Xie, X.J., Zhang, L.P. and Guo, W. (2013) Hydrogeochemistry of high iodine groundwater: a case study at the Datong Basin, northern China. Environ Sci-Proc Imp 15, 848-859.

Li, J.X., Zhou, H.L., Wang, Y.X., Xie, X.J. and Qian, K. (2017) Sorption and speciation of iodine in groundwater system: The roles of organic matter and organic-mineral complexes. Journal of Contaminant Hydrology 201, 39-47.

Li, W.J. and Tao, Z.Y. (2003) Comparative study on Np(V) sorption on oxides of aluminum and silicon: effects of humic substance and carbonate in solution. Journal of Colloid and Interface Science 267, 25-31.

Lindahl, P., Roos, P., Holm, E. and Dahlgaard, H. (2005) Studies of Np and Pu in the marine environment of Swedish-Danish waters and the North Atlantic Ocean. Journal of Environmental Radioactivity 82, 285-301.

Liu, Y. and Gunten, H.R.v. (1988) Migration chemistry and behaviour of iodine relevant to geological disposal of radioactive wastes A literature review with a compilation of sorption data, Switzerland, p. 183.

Lu, N., Cotter, C.R., Kitten, H.D., Bentley, J. and Triay, I.R. (1998) Reversibility of sorption of plutonium-239 onto hematite and goethite colloids. Radiochimica Acta 83, 167-173.

Lu, N.P., Reimus, P.W., Parker, G.R., Conca, J.L. and Triay, I.R. (2003) Sorption kinetics and impact of temperature, ionic strength and colloid concentration on the adsorption of plutonium-239 by inorganic colloids. Radiochimica Acta 91, 713-720.

Lukashenko, S., Kabdyrakova, A., Lind, O.C., Gorlachev, I., Kunduzbayeva, A., Kvochkina, T., Janssens, K., De Nolf, W., Yakovenko, Y. and Salbu, B. (2020) Radioactive particles released from different sources in the Semipalatinsk Test Site. Journal of Environmental Radioactivity 216.

Machesky, M.L., Bischoff, B.L. and Anderson, M.A. (1989) Calorimetric Investigation of Anion Adsorption onto Goethite. Environmental Science & Technology 23, 580-587.

Maher, K., Bargar, J.R. and Brown, G.E., Jr. (2013) Environmental Speciation of Actinides. Inorganic chemistry 52, 3510-3532.

McBeth, J.M., Lear, G., Lloyd, J.R., Livens, F.R., Morris, K. and Burke, I.T. (2007) Technetium reduction and reoxidation in aquifer sediments. Geomicrobiology Journal 24, 189-197.

McCubbin, D. and Leonard, K.S. (1996) Photochemical dissolution of radionuclides from marine sediments. Marine Chemistry 55, 399-408.

McCubbin, D., Leonard, K.S. and Emerson, H.S. (2002) Influence of thermal and photochemical reactions upon the redox cycling of Pu between solid and solution phases in seawater. Marine Chemistry 80, 61-77.

Micheau, C., Virot, M., Dourdain, S., Dumas, T., Menut, D., Solari, P.L., Venault, L., Diat, O., Moisy, P. and Nikitenko, S.I. (2020) Relevance of formation conditions to the size, morphology and local structure of intrinsic plutonium colloids. Environmental Science: Nano.

Mironenko, M.V., Malikov, D.A., Kulyako, Y.M. and Myasoedov, B.F. (2006) Sorption of Np(V) on montmorillonite from solutions of MgCl2 and CaCl2. Radiochemistry 48, 69-74.

Missana, T., Alonso, U., Garcia-Gutierrez, M. and Mingarro, M. (2008) Role of bentonite colloids on europium and plutonium migration in a granite fracture. Applied Geochemistry 23, 1484-1497.

Moon, H.S., Komlos, J. and Jaffe, P.R. (2007) Uranium reoxidation in previously bioreduced sediment by dissolved oxygen and nitrate. Environmental Science & Technology 41, 4587-4592.

Moore, R.C., Pearce, C.I., Morad, J., Chatterjee, S., Levitskaia, T.G., Asmussen, R.M., Lawter, A.R., Neeway, J.J., Qafoku, N.P., Rigali, M.J., Saslow, S.A., Szecsody, J.E., Thallapally, P.K., Wang, G.H. and Freedman, V.L. (2020) Iodine immobilization by materials through sorption and redox-driven processes: A literature review. Science of the Total Environment 716.

Moreau, L.M., Herve, A., Straub, M.D., Russo, D.R., Abergel, R.J., Alayoglu, S., Arnold, J., Braun, A., Deblonde, G.J.P., Liu, Y., Lohrey, T.D., Olive, D.T., Qiao, Y., Rees, J.A., Shuh, D.K., Teat, S.J., Booth, C.H. and Minasian, S.G. (2020) Structural properties of ultra-small thorium and uranium dioxide nanoparticles embedded in a covalent organic framework. Chemical Science 11, 4648-4668.

Muller, K., Foerstendorf, H., Brendler, V. and Bernhard, G. (2009) Sorption of Np(V) onto TiO2, SiO2, and ZnO: An in Situ ATR FT-IR Spectroscopic Study. Environmental Science & Technology 43, 7665-7670.

Muller, K., Groschel, A., Rossberg, A., Bok, F., Franzen, C., Brendler, V. and Foerstendorf, H. (2015) In situ Spectroscopic Identification of Neptunium(V) Inner-Sphere Complexes on the Hematite-Water Interface. Environmental Science & Technology 49, 2560-2567.

Muramatsu, Y., Uchida, S., Sriyotha, P. and Sriyotha, K. (1990) Some Considerations on the Sorption and Desorption Phenomena of Iodide and Iodate on Soil. Water Air Soil Pollut. 49, 125-138.

Nagasaki, S., Tanaka, S. and Suzuki, A. (1999) Sorption of neptunium on bentonite and its migration in geosphere. Colloid Surface A 155, 137-143.

Nagata, T. and Fukushi, K. (2010) Prediction of iodate adsorption and surface speciation on oxides by surface complexation modeling. Geochimica Et Cosmochimica Acta 74, 6000-6013.

Nagata, T., Fukushi, K. and Takahashi, Y. (2009) Prediction of iodide adsorption on oxides by surface complexation modeling with spectroscopic confirmation. Journal of Colloid and Interface Science 332, 309-316.

Nakata, K., Nagasaki, S., Tanaka, S., Sakamoto, Y., Tanaka, T. and Ogawa, H. (2000) Sorption and desorption kinetics of Np(V) on magnetite and hematite. Radiochimica Acta 88, 453-457.

Nakata, K., Nagasaki, S., Tanaka, S., Sakamoto, Y., Tanaka, T. and Ogawa, H. (2002) Sorption and reduction of neptunium(V) on the surface of iron oxides. Radiochimica Acta 90, 665-669.

Nakata, K., Nagasaki, S., Tanaka, S., Sakamoto, Y., Tanaka, T. and Ogawa, H. (2004) Reduction rate of neptunium(V) in heterogeneous solution with magnetite. Radiochimica Acta 92, 145-149.

Neal, C. and Truesdale, V.W. (1976) The sorption of iodate and iodide by riverine sediments: its implications to dilution gauging and hydrochemistry of iodine. Journal of Hydrology 31, 281-291.

Neck, V., Altmaier, M., Seibert, A., Yun, J.I., Marquardt, C.M. and Fanghaenel, T. (2007) Solubility and redox reactions of Pu(IV) hydrous oxide: Evidence for the formation of PuO2+x(s, hyd). Radiochimica Acta 95, 193-207.

Neck, V., Kim, J.I., Seidel, B.S., Marquardt, C.M., Dardenne, K., Jensen, M.P. and Hauser, W. (2001) A spectroscopic study of the hydrolysis, colloid formation and solubility of Np(IV). Radiochimica Acta 89, 439-446.

Newsome, L., Morris, K. and Lloyd, J.R. (2014) The biogeochemistry and bioremediation of uranium and other priority radionuclides. Chemical Geology 363, 164-184.

Nichols, A.L. and Verpelli, M. (2007) Handbook of nuclear data for safeguards, International Atomic Energy Agency (IAEA), p. 94.

Niitsu, Y., Sato, S., Ohashi, H., Sakamoto, Y., Nagao, S., Ohnuki, T. and Muraoka, S. (1997) Effects of humic acid on the sorption of neptunium(V) on kaolinite. Journal of Nuclear Materials 248, 328-332.

Novikov, A.P., Kalmykov, S.N., Utsunomiya, S., Ewing, R.C., Horreard, F., Merkulov, A., Clark, S.B., Tkachev, V.V. and Myasoedov, B.F. (2006) Colloid transport of plutonium in the far-field of the Mayak Production Association, Russia. Science 314, 638-641.

OECD (1989) Plutonium fuel : an assessment. Organisation for Economic Co-operation and Development ; OECD Publications and Information Centre, distributor], Paris : [Washington, D.C.

Ojovan, M.I. and Lee, W.E. (2014) 10 - Long-Lived Waste Radionuclides, in: Ojovan, M.I., Lee, W.E. (Eds.), An Introduction to Nuclear Waste Immobilisation (Second Edition). Elsevier, Oxford, pp. 107-115.

Panak, P.J., Booth, C.H., Caulder, D.L., Bucher, J.J., Shuh, D.K. and Nitsche, H. (2002) X-ray absorption fine structure spectroscopy of plutonium complexes with Bacillus sphaericus. Radiochimica Acta 90, 315-321.

Pathak, P.N. and Choppin, G.R. (2007) Sorption of neptunyl(V) cations on suspended silicate: Effects of pH, ionic strength, complexing anions, humic acid, and metal ions. Journal of Radioanalytical and Nuclear Chemistry 274, 53-60.

Peak, D. and Sparks, D.L. (2002) Mechanisms of selenate adsorption on iron oxides and hydroxides. Environmental Science & Technology 36, 1460-1466.

Pidchenko, I., März, J., Hunault, M.O.J.Y., Bauters, S., Butorin, S.M. and Kvashnina, K.O. (2020) Synthesis, Structural, and Electronic Properties of K4PuVIO2(CO3)3(cr): An Environmentally Relevant Plutonium Carbonate Complex. Inorganic Chemistry 59, 11889-11893.

Powell, B.A., Dai, Z.R., Zavarin, M., Zhao, P.H. and Kersting, A.B. (2011) Stabilization of plutonium nano-colloids by epitaxial distortion on mineral surfaces. Environmental Science & Technology 45, 2698-2703.

Powell, B.A., Fjeld, R.A., Kaplan, D.I., Coates, J.T. and Serkiz, S.M. (2004) $Pu(V)O_2^+$ adsorption and reduction by synthetic magnetite (Fe_3O_4). Environmental Science & Technology 38, 6016-6024.

Powell, B.A., Fjeld, R.A., Kaplan, D.I., Coates, J.T. and Serkiz, S.M. (2005) $Pu(V)O_2^+$ adsorption and reduction by synthetic hematite and goethite. Environmental Science & Technology 39, 2107-2114.

Qafoku, N.P., Bagwell, C.E., Lawter, A.R., Truex, M.J., Szecsody, J.E., Qafoku, O., Kovarik, L., Zhong, L., Mitroshkov, A.V. and Freedman, V.L. (2018) Conceptual Model of Subsurface Processes for Iodine at the Hanford Site, United States.

Reeder, R.J., Nugent, M., Lamble, G.M., Tait, C.D. and Morris, D.E. (2000) Uranyl incorporation into calcite and aragonite: XAFS and luminescence studies. Environmental Science & Technology 34, 638-644.

Reeder, R.J., Nugent, M., Tait, C.D., Morris, D.E., Heald, S.M., Beck, K.M., Hess, W.P. and Lanzirotti, A. (2001) Coprecipitation of uranium(VI) with calcite: XAFS, micro-XAS, and luminescence characterization. Geochimica et Cosmochimica Acta 65, 3491-3503.

Reiller, P., Moulin, V., Casanova, F. and Dautel, C. (2002) Retention behaviour of humic substances onto mineral surfaces and consequences upon thorium (IV) mobility: case of iron oxides. Applied Geochemistry 17, 1551-1562.

Righetto, L., Bidoglio, G., Azimonti, G. and Bellobono, I.R. (1991) Competitive Actinide Interactions in Colloidal Humic-Acid Mineral Oxide Systems. Environmental Science & Technology 25, 1913-1919.

Riglet, C., Robouch, P. and Vitorge, P. (1989) Standard Potentials of the (Mo22+/Mo2+) and (M4+/M3+) Redox Systems for Neptunium and Plutonium. Radiochimica Acta 46, 85-94.

Roberts, H., Morris, K., Mosselmans, J., Law, G. and Shaw, S. (2019) Neptunium Reactivity During Co-Precipitation and Oxidation of Fe(II)/Fe(III) (Oxyhydr)oxides. Geosciences 9.

Romanchuk, A.Y., Kalmykov, S.N. and Aliev, R.A. (2011) Plutonium sorption onto hematite colloids at femto- and nanomolar concentrations. Radiochimica Acta 99, 137-144.

Rovnyi, S.I., Sokhina, L.P. and Goncharuk, L.V. (2006) Coprecipitation of neptunium(IV) and plutonium(IV) with hydrolyzed iron(III) in carbonate solutions. Radiochemistry 48, 482-485.

Runde, W., Bean, A.C., Albrecht-Schmitt, T.E. and Scott, B.L. (2003) Structural characterization of the first hydrothermally synthesized plutonium compound, PuO2(IO3)(2)center dot H2O. Chemical Communications, 478-479.

Runde, W., Conradson, S.D., Efurd, D.W., Lu, N.P., VanPelt, C.E. and Tait, C.D. (2002) Solubility and sorption of redox-sensitive radionuclides (Np, Pu) in J-13 water from the Yucca Mountain site: comparison between experiment and theory. Applied Geochemistry 17, 837-853.

Saiers, J.E. and Hornberger, G.M. (1996) The role of colloidalkaolinite in the transport of cesium through laboratory sand columns. Water Resources Research 32, 33-41.

Sakamoto, Y., Nagao, S., Ogawa, H. and Rao, R.R. (2000) The migration behavior of Np(V) in sandy soil and granite media in the presence of humic substances. Radiochimica Acta 88, 651-656.

Sanchez, A.L., Murray, J.W. and Sibley, T.H. (1985) The adsorption of plutonium IV and V on goethite. Geochimica Et Cosmochimica Acta 49, 2297-2307.

Schmeide, K. and Bernhard, G. (2009) Redox stability of neptunium(V) and neptunium(IV) in the presence of humic substances of varying functionality. Radiochimica Acta 97, 603-611.

Schmeide, K. and Bernhard, G. (2010) Sorption of Np(V) and Np(IV) onto kaolinite: Effects of pH, ionic strength, carbonate and humic acid. Applied Geochemistry 25, 1238-1247.

Schwehr, K.A., Santschi, P.H., Kaplan, D.I., Yeager, C.M. and Brinkmeyer, R. (2009) Organo-Iodine Formation in Soils and Aquifer Sediments at Ambient Concentrations. Environmental Science & Technology 43, 7258-7264.

Serne, R.J., LeGore, V.L., Cantrell, K.J., Lindenmeier, C.W., Campbell, J.A., Amonette, J.E., Conca, J.L. and Wood, M.I. (1993) Solid-waste leach characteristics and contaminant-sediment interactions. Volume 1, Batch leach and adsorption tests and sediment characterization, United States.

Shaughnessy, D.A., Nitsche, H., Booth, C.H., Shuh, D.K., Waychunas, G.A., Wilson, R.E., Gill, H., Cantrell, K.J. and Serne, R.J. (2003) Molecular interfacial reactions between Pu(VI) and manganese oxide minerals manganite and hausmannite. Environmental Science & Technology 37, 3367-3374.

Shcherbina, N.S., Perminova, I.V., Kalmykov, S.N., Kovalenko, A.N., Haire, R.G. and Novikov, A.P. (2007) Redox and complexation interactions of neptunium(V) with quinonoid-enriched humic derivatives. Environmental Science & Technology 41, 7010-7015.

Smith, D.K., Finnegan, D.L. and Bowen, S.M. (2003) An inventory of long-lived radionuclides residual from underground nuclear testing at the Nevada test site, 1951-1992. Journal of Environmental Radioactivity 67, 35-51.

Smith, K.F., Bryan, N.D., Swinburne, A.N., Bots, P., Shaw, S., Natrajan, L.S., Mosselmans, J.F.W., Livens, F.R. and Morris, K. (2015) U(VI) behaviour in hyperalkaline calcite systems. Geochimica Et Cosmochimica Acta 148, 343-359.

Smith, K.F., Morris, K., Law, G.T.W., Winstanley, E.H., Livens, F.R., Weatherill, J.S., Abrahamsen-Mills, L.G., Bryan, N.D., Mosselmans, J.F.W., Cibin, G., Parry, S., Blackham, R., Law, K.A. and Shaw, S. (2019) Plutonium(IV) Sorption during Ferrihydrite Nanoparticle Formation. ACS Earth and Space Chemistry.

Snow, M.S., Zhao, P., Dai, Z., Kersting, A.B. and Zavarin, M. (2013) Neptunium(V) sorption to goethite at attomolar to micromolar concentrations. Journal of Colloid and Interface Science 390, 176-182.

Strickland, C.E., Johnson, C.D., Lee, B.D., Qafoku, N., Szecsody, J.E., Truex, M.J. and Vermeul, V.R. (2017) Identification of Promising Remediation Technologies for Iodine in the UP-1 Operable Unit, United States.

Sturchio, N.C., Antonio, M.R., Soderholm, L., Sutton, S.R. and Brannon, J.C. (1998) Tetravalent uranium in calcite. Science 281, 971-973.

Su, C.M. and Suarez, D.L. (2000) Selenate and selenite sorption on iron oxides: An infrared and electrophoretic study. Soil Science Society of America Journal 64, 101-111.

Takahashi, Y., Minai, Y., Ambe, S., Makide, Y. and Ambe, F. (1999) Comparison of adsorption behavior of multiple inorganic ions on kaolinite and silica in the presence of humic acid using the multitracer technique. Geochimica Et Cosmochimica Acta 63, 815-836.

Teterin, A.Y., Maslakov, K.I., Teterin, Y.A., Kalmykov, S.N., Ivanov, K.E., Vukcevic, L., Khasanova, A.B. and Shcherbina, N.S. (2006) Interaction of neptunyl with goethite (alpha-FeOOH), maghemite (gamma-Fe2O3), and hematite (alpha-Fe2O3) in water as probed by X-ray photoelectron spectroscopy. Russ J Inorg Chem+ 51, 1937-1944.

Ticknor, K.V. and Cho, Y.H. (1990) Interaction of Iodide and Iodate with Granitic Fracture-Filling Minerals. J Radioan Nucl Ch Ar 140, 75-90.

Tinnacher, R.M., Zavarin, M., Powell, B.A. and Kersting, A.B. (2011) Kinetics of neptunium(V) sorption and desorption on goethite: An experimental and modeling study. Geochimica Et Cosmochimica Acta 75, 6584-6599.

Tochiyama, O., Yamazaki, H. and Mikami, T. (1996) Sorption of neptunium(V) on various aluminum oxides and hydrous aluminum oxides. Radiochimica Acta 73, 191-198.

Truex, M.J., Lee, B.D., Johnson, C.D., Qafoku, N., Szecsody, J.E., Kyle, J.E., Tfaily, M.M., Snyder, M.M.V., Cantrell, K.J., Saunders, D.L., Lawter, A.R., Oostrom, M.L., Tartakovsky, G.D., Leavy, I.I., McElroy, E.M., Appriou, D., Sahajpal, R., Carroll, M.M., Chu, R.K., Cordova, E., Last, G.V., Lee, H., Kaplan, D.I., Garcia, W.L., Kerisit, S.N., Qafoku, O., Bowden, M.E., Smith, F.N., Toyoda, J.G. and Plymale, A.E. (2017) Conceptual Model of Iodine Behavior in the Subsurface at the Hanford Site, United States.

Turner, D.R., Pabalan, R.T. and Bertetti, F.P. (1998) Neptunium(V) sorption on montmorillonite: An experimental and surface complexation modeling study. Clay Clay Min. 46, 256-269.

Wang, G.H., Qafoku, N.P., Szecsody, J.E., Strickland, C.E., Brown, C.F. and Freedman, V.L. (2019) Time-Dependent Iodate and Iodide Adsorption to Fe Oxides. Acs Earth and Space Chemistry 3, 2415-2420.

Wang, P.M., Anderko, A. and Turner, D.R. (2001) Thermodynamic modeling of the adsorption of radionuclides on selected minerals. I: Cations. Industrial & Engineering Chemistry Research 40, 4428-4443.

Wang, S.A., Villa, E.M., Diwu, J.A., Alekseev, E.V., Depmeier, W. and Albrecht-Schmitt, T.E. (2011) Role of Anions and Reaction Conditions in the Preparation of Uranium(VI), Neptunium(VI), and Plutonium(VI) Borates. Inorganic Chemistry 50, 2527-2533.

Whitehead, D.C. (1974) The sorption of iodide by soil components. Journal of the Science of Food and Agriculture 25, 73-79.

Whitehead, D.C. (1984) The Distribution and Transformations of Iodine in the Environment. Environment International 10, 321-339.

Wu, T., Amayri, S. and Reich, T. (2009) Neptunium(V) sorption onto gibbsite. Radiochimica Acta 97, 99-103.

Wylie, E.M., Olive, D.T. and Powell, B.A. (2016) Effects of Titanium Doping in Titanomagnetite on Neptunium Sorption and Speciation. Environmental Science & Technology 50, 1853-1858.

Xu, C., Kaplan, D.I., Zhang, S.J., Athon, M., Ho, Y.F., Li, H.P., Yeager, C.M., Schwehr, K.A., Grandbois, R., Wellman, D. and Santschi, P.H. (2015) Radioiodine sorption/desorption and speciation transformation by subsurface sediments from the Hanford Site. Journal of Environmental Radioactivity 139, 43-55.

Yang, C.L., Powell, B.A., Zhang, S.D. and Rao, L.F. (2015) Surface complexation modeling of neptunium(V) sorption to lepidocrocite (gamma-FeOOH). Radiochimica Acta 103, 707-717.

Yu, Z.S., Warner, J.A., Dahlgren, R.A. and Casey, W.H. (1996) Reactivity of iodide in volcanic soils and noncrystalline soil constituents. Geochimica Et Cosmochimica Acta 60, 4945-4956.

Zavarin, M., Powell, B.A., Bourbin, M., Zhao, P. and Kersting, A.B. (2012) Np(V) and Pu(V) Ion Exchange and Surface-Mediated Reduction Mechanisms on Montmorillonite. Environ. Sci. Technol. 46, 2692-2698.

Zavarin, M., Roberts, S.K., Hakem, N., Sawvel, A.M. and Kersting, A.B. (2005) Eu(III), Sm(III), Np(V), Pu(V), and Pu(IV) sorption to calcite. Radiochimica Acta 93, 93-102.

Zeh, P., Kim, J.I., Marquardt, C.M. and Artinger, R. (1999) The reduction of Np(V) in groundwater rich in humic substances. Radiochimica Acta 87, 23-28.

Zhang, S., Du, J., Xu, C., Schwehr, K.A., Ho, Y.F., Li, H.P., Roberts, K.A., Kaplan, D.I., Brinkmeyer, R., Yeager, C.M., Chang, H.S. and Santschi, P.H. (2011) Concentration-Dependent Mobility, Retardation, and Speciation of Iodine in Surface Sediment from the Savannah River Site. Environmental Science & Technology 45, 5543-5549.

Zhao, P.H., Begg, J.D., Zavarin, M., Tumey, S.J., Williams, R., Dai, Z.R.R., Kips, R. and Kersting, A.B. (2016) Plutonium(IV) and (V) Sorption to Goethite at Sub-Femtomolar to Micromolar Concentrations: Redox Transformations and Surface Precipitation. Environmental Science & Technology 50, 6948-6956.

Zhao, P.H., Zavarin, M., Leif, R.N., Powell, B.A., Singleton, M.J., Lindvall, R.E. and Kersting, A.B. (2011) Mobilization of actinides by dissolved organic compounds at the Nevada Test Site. Applied Geochemistry 26, 308-318.